ATR

AUSTRALIAN TELECOMMUNICATION RESEARCH

Volume 11, Number 3, 1977

A.T.R. is issued normally twice a year (in May and November) by the Telecommunication Society of Australia. Each volume comprises two regular numbers issued in one calendar year.

Subscriptions for A.T.R. may be placed with the General Secretary, Telecommunication Society of Australia, Box 4050, G.P.O., Melbourne, Victoria, Australia, 3001. The subscription rates are detailed below. All rates are post free. Remittances should be made payable to the Telecommunications Society of Australia.

Contributions to A.T.R. should be addressed to: Secretary of Editorial Board, Australian Telecommunication Research, Telecom Australia Research Laboratories, 59 Little Collins Street, Melbourne, Australia 3000.

ATR
AUSTRALIAN TELECOMMUNICATION RESEARCH

Volume 11, Number 3, 1977

Contents

Albert Jakob Seyler: 1913-1977

On 26 April 1977, those working in the telecommunications field were saddened to hear of the passing of Dr. Seyler.

Albert J. Seyler was born in Germany on 24 July 1913, and qualified as Diplom Ingenieur at the Technical University of Munich with Honours in 1938. During the next ten years, he was engaged in research on air navigational aids, radar and radar counter measures, a field in which he added very significantly indeed to both the knowledge and techniques available at that time.

In 1948, he emigrated to Australia where he joined the P.M.G. Research Laboratories as a technical expert. He was immediately placed in charge of the Pulse Techniques Division, where he developed many technical performance standards and measurement techniques necessary for the successful introduction of television into Australia. He then developed an interest in the reduction of bandwidth necessary for television transmission, which naturally led him into an interest in the psycho-physical aspects of human behaviour, and the coding and processing of visual information with particular emphasis on the interaction of human visual perception with the engineering visual communication systems. He carried out early pioneering work in the fields of delay detail perception and difference coding, for both frame and line. This work earned him the degree of Master of Electrical Engineering at Melbourne University in 1956, on the basis of his published work. In 1966, he was awarded the degree of Dr. of Applied Science by Melbourne University, again for his published work in this field. In 1964, he became Head of the Advanced Techniques Branch, where he directed research in the fields of Guided and Unguided Media, Computer Applications, Solid State and Quantum Electronics and Visual Communications. In recent years, Dr. Seyler's personal research interests centred on man-technology interaction problems in telecommunication and on the psychological and social impact of such systems on human communication and the future life-style of society. In December 1968, Dr. Seyler commenced some long service leave, during which he took a position of a consultant for three months at Holmdel in the United States with Bell Telephone Laboratories, where he furthered his studies in human communications. In 1973, he took a position for a period of three months as a consultant at Ottowa with Bell Northern Research, where he studied the fundamental human aspects of both audio and visual teleconferencing. His particular interest at that time was in extending previous theories involving two people to groups of people.

Apart from his position as Assistant Director, Advanced Techniques, of the Telecom Australia Research Laboratories, Dr. Seyler was also a member of the Faculty of Engineering of Monash University and Honorary Consultant in Communication Engineering at the University of Adelaide. He was a Fellow of the Australian Academy of Technological Science and also a Fellow and past President of the Institution of Radio and Electronics Engineers of Australia.

Challenge . . .

The Australian Government has recently awarded a contract for future supply of telephone exchanges utilising stored program control. The introduction of SPC exchanges into the local network will clear the way for the speedy introduction of new facilities for both the subscribers and Telecom Australia. This will be on a quite different basis from the past, as new facilities can be introduced on a near simultaneous basis very swiftly through the medium of program changes. This contrasts with the previous situation, in which changes necessarily took a long time to implement, as they required a considerable amount of modification of working equipment in the field.

This change of approach will not only have an impact for the subscriber, but it is also going to have an impact in ways of working for Telecom Australia. This will occur particularly in the fields of marketing, operating and in the theoretical work underlying basic planning.

In the past, the marketers have had a somewhat cloistered existence in an environment in which they were prisoners of the massive efforts needed to modify the network to introduce new facilities. When the application of stored program control is widespread, they will have a new flexibility and freedom to introduce new facilities. However, in the current situation in which the introduction of new facilities is a somewhat ponderous procedure, they have had little opportunity to gain experience in the selection of new facilities, or in their marketing. This is an aspect which will require considerable preliminary work before the use of SPC techniques become widespread if both the subscribers and Telecom Australia are to derive the maximum benefit from the use of SPC techniques.

Operating staff will be confronted with a different type of system; one-at-a-time operation of devices, switches, sub-systems, etc., will no longer be the norm. The control processes will have become invisible and will be handling many calls simultaneously. This invisibility will require the development of new tools, new procedures, and most importantly, new outlooks by maintenance staff. It will also require increased discipline in the control of unauthorised system modifications, even if for no other reason than to discourage the ardent fiddler who knows that his fiddling cannot be seen; further, if he has cured a mal-function, there will be no reason to suspect fiddling has taken place, but subsequent design work may have been compromised due to the existence of non-standard software.

The introduction of stored program control techniques on a large scale will bring a variety of challenges in its wake; many of these will be more involved with human rather than technical matters. This is part of an evolving pattern which is slowly gathering momentum and presenting a rather more subtle yet more pervasive challenge in its own right than that which has been posed in the past by purely technical matters.

The Effects of Excitation Conditions on Fibre Launching and Coupling Losses

G. P. KIDD*
Telecom Australia Research Laboratories

A straightforward geometrical optics method has been used to calculate the launching and coupling losses between source and fibre or between two fibres, taking into account all possible variations of source and fibre parameters likely to be met in practice. It is shown that the coupling losses between fibres are significantly less if the exciting fibre has a near-field power intensity distribution concentrated towards the centre of the fibre relative to the losses if equal excitation of all modes is assumed. Furthermore the losses due to diameter variations at a joint are considerably reduced for this form of intensity distribution. It is also shown that the launching efficiency between a stripe geometry injection laser and an arbitrary profile fibre may, with reasonable accuracy, be determined by assuming a symmetric source having near- and far-field characteristics appropriate to the major axis of the laser junction.

1. INTRODUCTION

Over the years a number of papers have investigated the efficiency of launching energy into optical fibres from a variety of sources (most recently for example Refs. 1, 2 and 3). In general these have imposed certain constraints on the source, usually by assuming a uniform power intensity distribution. Likewise other papers (eg Refs. 4, 5, 9) have studied coupling losses between fibres, but again with some constraints. Gloge (Ref. 4) comes closest to the practical situation by considering the effects of various power distributions in the exciting fibre as might occur as a result of mode mixing, but limits his analysis to coupling between two fibres of equal core diameter with no air gap between them.

It seems that a straightforward method of calculating both launching and coupling efficiencies is needed which takes into account all the possible variations of source and fibre parameters likely to be met in practice. This paper presents such a method based on geometrical optics. Since numerical integration is used in calculating the results the method is very general, so that completely arbitrary refractive index profiles and power intensity distributions can be analysed, if required. In this paper, however, parametric expressions for the intensity distribution $I(\ell)$ and refractive index profile $n(r)$ have been used to simplify the presentation of results.

The parameters considered are the effective diameter of the source or the exciting fibre and the shape of the intensity distribution; the far field radiation pattern; the index profile of the fibre or fibres (not necessarily the same); the diameter of the exciting fibre relative to the excited fibre; the spacing and offset between source and fibre or between two fibres; and the refractive index of the intermediate medium. The effects of tilts have not been considered, but could be included by an extension of the geometrical analysis. Likewise Fresnel reflection losses have been ignored, but could be taken into account in a straightforward manner (Ref.2).

2. COUPLING EFFICIENCY BETWEEN SOURCE AND FIBRE

2.1 On-axis Launching

The situation to be analysed is illustrated in Fig 1, where the effective source diameter B and the source-fibre spacing D have been normalized to the core radius. Both the source intensity distribution $I(\ell)$ and the index profile $n(r)$ are assumed circularly symmetric with their centres on axis.

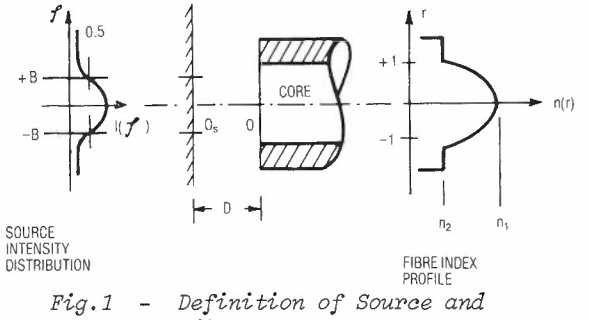

Fig.1 - Definition of Source and Fibre Parameters.

* This paper was written while the author was at the British Post Office Research Centre, Martlesham Heath.

To achieve a measure of generality the source intensity distribution is taken to be of the form

$$I(\ell) = \frac{A_1}{A_2+e^{C(\ell-B)}}$$

where $A_1 = 1-e^{-CB}$

$$A_2 = 1-2e^{-CB} \qquad (1)$$

Thus $I(\ell=B) = 0.5\ I(0)$

By selecting different values of B and C it is possible to represent a range of distributions of different effective diameters and shapes. A large value of C, for example, approximates a uniform distribution while a value of C=4 gives a parabolic shape. Further, to take account of different far field radiation patterns from various sources, it is assumed that the flux emitted from a point on the source varies as $\cos^m\phi$, where m=1 represents a Lambertian point source as might be expected for a LED, and higher values of m could be used to describe the more directional radiation of a laser diode for example.

The flux emitted from an elemental area ds at radius ℓ into a cone of half-angle ϕ is (Ref 6)

$$\Delta P = \int_0^{\phi} I(\ell)\cos^m\phi\ 2\pi\sin\phi\ d\phi\ ds$$

The total flux emitted from this elemental area into the forward hemisphere is then

$$\Delta P = 2\pi\ I(\ell)\int_0^{\frac{\pi}{2}} \cos^m\phi\ \sin\phi\ d\phi\ ds$$

$$= \frac{2\pi}{m+1}\ I(\ell)\ ds \qquad (2)$$

The flux from an elemental ring of width $d\ell$ at radius ℓ is given by

$$\frac{2\pi}{m+1}\ I(\ell)\ 2\pi\ell\ d\ell,$$

so that the total flux or power emitted by the source is

$$P_{tot} = \frac{4\pi^2}{m+1}\int_0^{\infty} I(\ell)\ell\, d\ell$$

For the intensity distribution (1) this gives

$$P_{tot} = \frac{4\pi^2}{m+1}\ \frac{(1-e^{-BC})}{(1-2e^{-BC})}\int_0^{\infty} \frac{\ell}{(1+be^{C\ell})}\ d\ell \qquad (3)$$

Where $b = \frac{1}{(e^{BC}-2)}$

The integral $\int_0^{\infty} \frac{\ell}{(1+be^{C\ell})}\ d\ell$

is not standard but can be reduced to

$$\frac{I_\infty}{C^2} = \left\{ \frac{[\log(e^{BC}-2)]^2}{2} + \sum_{i=1}^{\infty} \frac{(-1)^i}{i^2(e^{BC}-2)^i} + \sum_{i=1}^{\infty} \frac{(-1)^{i+1}}{i^2} \right\}$$

For a uniform source (ie large C) the total radiated power tends to

$$P_{tot} = \frac{2\pi^2}{m+1}\ B^2 \qquad (4)$$

If the intensity distribution is normalized to the total power P_{tot} the resultant distribution is

$$I_0(\ell) = \frac{(m+1)\ C^2}{(1+be^{\ell C})4\pi^2\ I_\infty} \qquad (5)$$

To calculate the launching efficiency it is necessary to determine the proportion of the total power that will be accepted into the fibre, and this of course is a function of the index profile, the source parameters, and the spacing between source and fibre. A completely arbitrary index profile could be assumed, but for the calculation of coupling efficiency it is probably sufficient to approximate a given profile by the so-called alpha-profile given by

$$n(r) = n_1\left(1-\frac{n_1-n_2}{n_1}\ r^{\alpha}\right), \quad 0 < r \leq 1$$

$$= n_2, \quad r > 1 \qquad (6)$$

As α goes from 2 to infinity the profile changes from parabolic towards the step-index form.

Consider a ray impinging on the fibre face at a point at radius r, with a local angle of incidence of θ_{za} (Fig 2). This ray will be refracted into the fibre, and its angle of refraction, from Snell's Law, will be given by

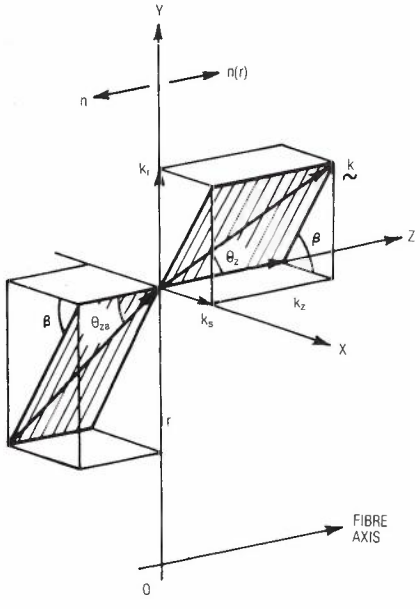

Fig.2 - Ray Vectors at Fibre Interface.

$$n(r)\sin\theta_z = n\sin\theta_{za}$$

where n(r) is the local refractive index of the fibre and n is the refractive index of the external medium (subsequently assumed to be unity). The plane of refraction makes an angle of $(\frac{\pi}{2} - \beta)$ to the radial direction.

Rays will be trapped if the angle θ_{za} is less than an angle I given by

$$\sin^2 I = n^2(r) - n_2^2$$

However other rays, the so-called leaky rays (Ref.7), can also propagate albeit with increased attenuation. The acceptance region for these rays is given by

$$\frac{n^2(r) - n_2^2}{1 - r^2\cos^2\beta} \geq \sin^2\theta_{za} > n^2(r) - n_2^2 \qquad (7)$$

Taking the left hand limit defines an elliptical excitation region for both trapped and leaky rays. Thus for a source-fibre spacing D (Fig 3) the major and minor radii are found by putting $\beta = 0$ and $\frac{\pi}{2}$ respectively, which gives for the minor radius

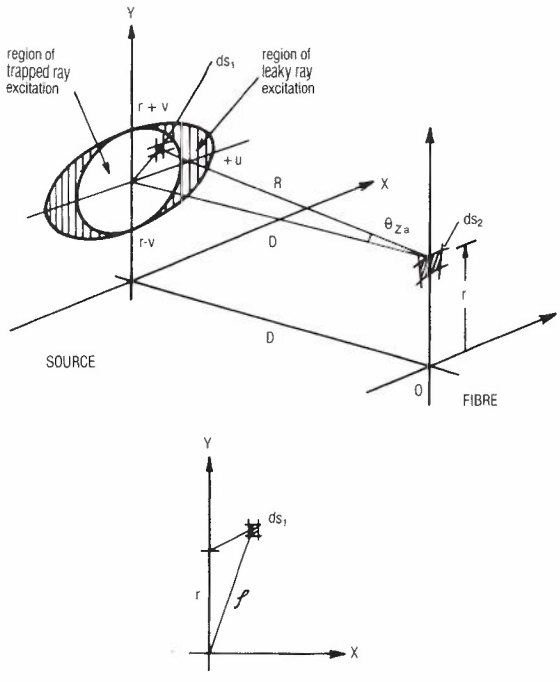

Fig.3 - Source Excitation Conditions.

$$v(r) = D\left\{\frac{n^2(r) - n_2^2}{1 - (n^2(r) - n_2^2)}\right\}^{\frac{1}{2}} \qquad (8a)$$

and for the major radius

$$u(r) = D\left\{\frac{n^2(r) - n_2^2}{(1-r^2) - (n^2(r) - n_2^2)}\right\}^{\frac{1}{2}}$$

$$= v(r)\left\{\frac{1 - (n^2(r) - n_2^2)}{(1-r^2)-(n^2(r)-n_2^2)}\right\}^{\frac{1}{2}} \qquad (8b)$$

If leaky rays are ignored then the excitation region on the source reduces to a circle of radius v(r).

We now require to calculate the power received by an elemental area ds_2 situated at radius r on the fibre face from the region of excitation defined above. Consider initially an elemental area ds_1 on the source, separated from ds_2 by a distance R and making an angle θ_{za} to it. The flux emitted from ds_1 per unit solid angle in the direction of ds_2 will then be

$$I(\ell)\cos^m\phi\, ds_1$$

Now ds_2 subtends a solid angle at ds_1 of

$$\frac{\cos\theta_{za}\, ds_2}{R^2}$$

so that the flux or power received by ds_2 from ds_1 is

$$dP(r) = \frac{I_0(\ell)\cos^{m+1}\theta_{za}}{R^2} \cdot ds_1 ds_2$$

The total power accepted from the source into ds_2 at r is therefore

$$\frac{dP(r)}{ds_2} = \int_{-u}^{u} \int_{y_1=\Psi_1(x)}^{y_2=\Psi_2(x)} \frac{I_0(x,y)\cos^{m+1}\theta_{za}}{R^2} \cdot dy\,dx \qquad (9)$$

where $\Psi_1(x)$ and $\Psi_2(x)$ are the appropriate limits imposed by the ellipse (or circle) defining the region of excitation.

Now $\cos\theta_{za} = \frac{D}{R}$

$$\text{and } R = \left\{ D^2 + x^2 + (y-r)^2 \right\}^{\frac{1}{2}}$$

$$\text{also } \ell = (x^2 + y^2)^{\frac{1}{2}}$$

Thus for the assumed intensity distribution

$$\frac{dP(r)}{ds_2} = \frac{(m+1)C^2}{4\pi^2 I_\infty D^2} \iint \frac{1}{1+be^{C(x^2+y^2)^{\frac{1}{2}}}} \left\{ \frac{D}{\left(D^2+x^2+(y-r)^2 \right)^{\frac{1}{2}}} \right\}^{m+3} dy\,dx \qquad (10)$$

Because of the assumed circular symmetry the power received by an elemental ring of thickness dr at radius r is then

$$P(r) = dP(r)\, 2\pi r\, dr$$

and the total power accepted by the fibre is

$$P_{acc} = 2\pi \int_0^1 dP(r)\, r\, dr \qquad (11)$$

Since the total radiated power from the source has been normalized to unity, P_{acc} therefore gives the required launching efficiency.

The launching efficiency has been calculated by numerical integration for fibres having alpha values ranging from 2 to 32, for excitation conditions representing those likely to be found with high radiance LED's and injection laser diodes. If it is assumed that the LED has an effective diameter equal to that of the core and that its intensity is uniform across most of the electroluminescent region, but falls off at the extremities, then an appropriate intensity distribution might be one with B = 1 and C = 20. Further, since this source is essentially Lambertian, the value of m will be 1. The launching loss with this source and fibres of numerical aperture 0.15 and 0.20 is shown in Fig 4. As expected the loss for a parabolic fibre is about 3 dB greater than for a step-index fibre. The additional loss of about 2.5 dB expected for a fibre with NA=0.15 over that for a fibre with NA=0.20 is also demonstrated.

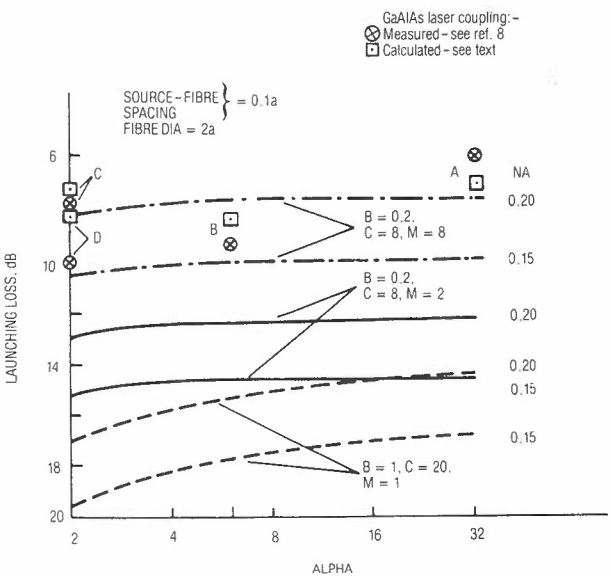

Fig.4 - Launching Losses as a Function of Profile and Excitation Conditions.

It is not so easy to represent semiconductor laser diodes because of their asymmetric near- and far-field characteristics. In the plane of the junction the near-field intensity will tend to be concentrated towards the centre and taper off towards the edges. The far-field radiation in this plane will be highly directional corresponding to a very high value of m, while that in the plane perpendicular to the junction will be more diffuse. Two sets of curves for an assumed near-field intensity given by B = 0.2 and C = 8 and far-field characteristics of m = 2 and m = 8 are given in Fig 4.

Benson et al (Ref 8) have measured the launching efficiencies from a stripe geometry GaAlAs laser diode into various fibres whose characteristics were as shown in Table 1.

TABLE 1 - Measured Launching Efficiencies (Ref. 8)

Fibre	Type	Alpha (assumed)	Core Dia	NA	Measured Launching Efficiency
A	step	32	55μm	0.171	24%
B	partially graded	6	50μm	0.148	13%
C	graded	2	46μm	0.171	17%
D	graded	2	42μm	0.162	10%

The radiation pattern of the laser diode used had an intensity of 0.8 at a half-angle of 10^0 in the plane perpendicular to the junction which corresponds to a value of m = 14. The junction dimensions were 15 μm x 0.5 μm. From knowledge of the behaviour of stripe geometry lasers it would seem reasonable to assume a half-intensity width of 10μm and a value of C = 8. The launching efficiencies calculated for each of the fibres, together with the measured values, are shown in Fig 4. It is seen that although the asymmetric source has been approximated by a symmetric one having the characteristics appropriate to the major axis of the junction, the differences between measured and calculated efficiencies are less than 1 dB for three of the fibres and about 2 dB for fibre D.

It should be noted that since the measurements of Ref 8 were carried out on short fibres (approximately 50 cm), the resulting efficiencies are probably greater than if much longer fibres had been used in which the leaky mode energy would have been negligible. The calculated efficiencies on the other hand exclude leaky rays and are therefore directly applicable to the long lengths of fibre likely to be found in practical systems.

2.2 Axial offset of source

Assume an axial offset d between the centre of symmetry O_s of the source and the centre O of the fibre. For an elemental area ds_2 displaced azimuthally an angle ξ from the Y axis of the fibre the general launching conditions will be as shown in Fig 5. If we rotate the X-Y axes through an angle ξ in the direction shown, then with reference to the new ordinates $[X^1,Y^1]$ the excitation conditions are similar to the situation considered in the previous section, except that ℓ corresponding to an arbitrary point (x^1,y^1) on the source will now be a function of ξ and d. If (x_s,y_s) defines the point in terms of the source ordinates then $\ell = (x_s^2 + y_s^2)^{\frac{1}{2}}$, and by appropriate transformation

$$x_s = x^1 \cos\xi - y^1 \sin\xi$$

$$y_s = x^1 \sin\xi + y^1 \cos\xi - d \qquad (12)$$

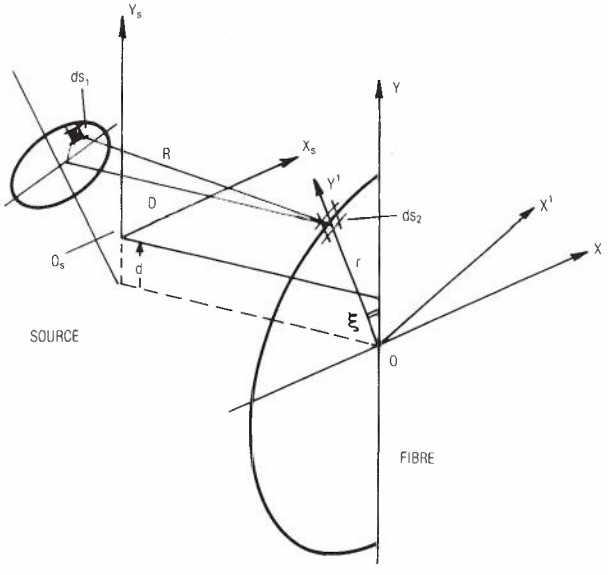

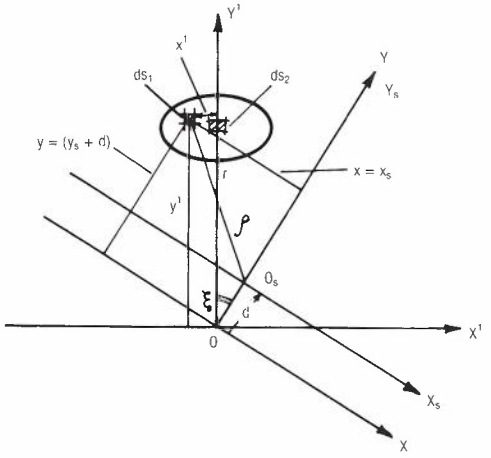

Fig.5 - Source Excitation Conditions for Offset Axes.

The power received by the elemental area ds_2 at radius r and angle ξ is then

$$\frac{dP(r,\xi)}{ds_2} = \frac{(m+1)\,C^2}{4\pi^2\, I_\infty\, D^2} \iint \frac{1}{1+be^{C(x_s^2+y_s^2)^{\frac{1}{2}}}}$$

$$\left\{ \frac{D}{\left[D^2 + x^{1^2} + (y^1 - r)^2\right]^{\frac{1}{2}}} \right\}^{m+3} dydx \qquad (13)$$

The total accepted power is

$$P_{acc}(d) = 2 \int_{r=0}^{1} \int_{\xi=0}^{\pi} r \, dP(r,\xi) \, d\xi \, dr \qquad (14)$$

which gives the launching efficiency for a given axial displacement d.

As in the previous section launching efficiencies have been calculated by numerical techniques for a number of source and fibre conditions. Two sources have been simulated: the first an LED having the values B = 1, C = 20 and m = 1, and the second an injection laser having the values B = 0.2, C = 8, m = 8. The launching efficiencies between these and a parabolic profile fibre (α = 2) and a step-index fibre (α = 32), as a function of offset and spacing, are presented in Figs 6 and 7. It is seen that as long as source-fibre spacing is not greater than (about) the core diameter, then offsets of at least 10% of the diameter (0.2a) can be tolerated without degrading the loss by more than 0.5 dB. As would be expected the step-index fibre excited by the laser is least sensitive to the influences of offset and spacing, while the parabolic fibre similarly excited is most sensitive to these effects.

Although a comparison in the previous section between certain measured and calculated on-axis launching efficiencies suggested that it may be reasonable to approximate the asymmetrical radiation characteristics of an injection laser by a symmetrical source, this may not hold for increased source-fibre spacings since the more directional radiation in the plane of the junction could then become dominant. If this were so, the measured efficiencies using a laser source would not fall off as rapidly as indicated in Fig 6 for increasing source-fibre spacing.

3. COUPLING LOSSES BETWEEN FIBRES

In this section we will adapt the preceding methods to calculate the coupling losses between two fibres of different core diameters and index profiles, and with their axes offset. Furthermore a near field intensity distribution for the exciting fibre of the form described earlier will be assumed in order to approximate those distributions likely to be found after long lengths of fibre.

The fibres will be assumed to have the following characteristics:

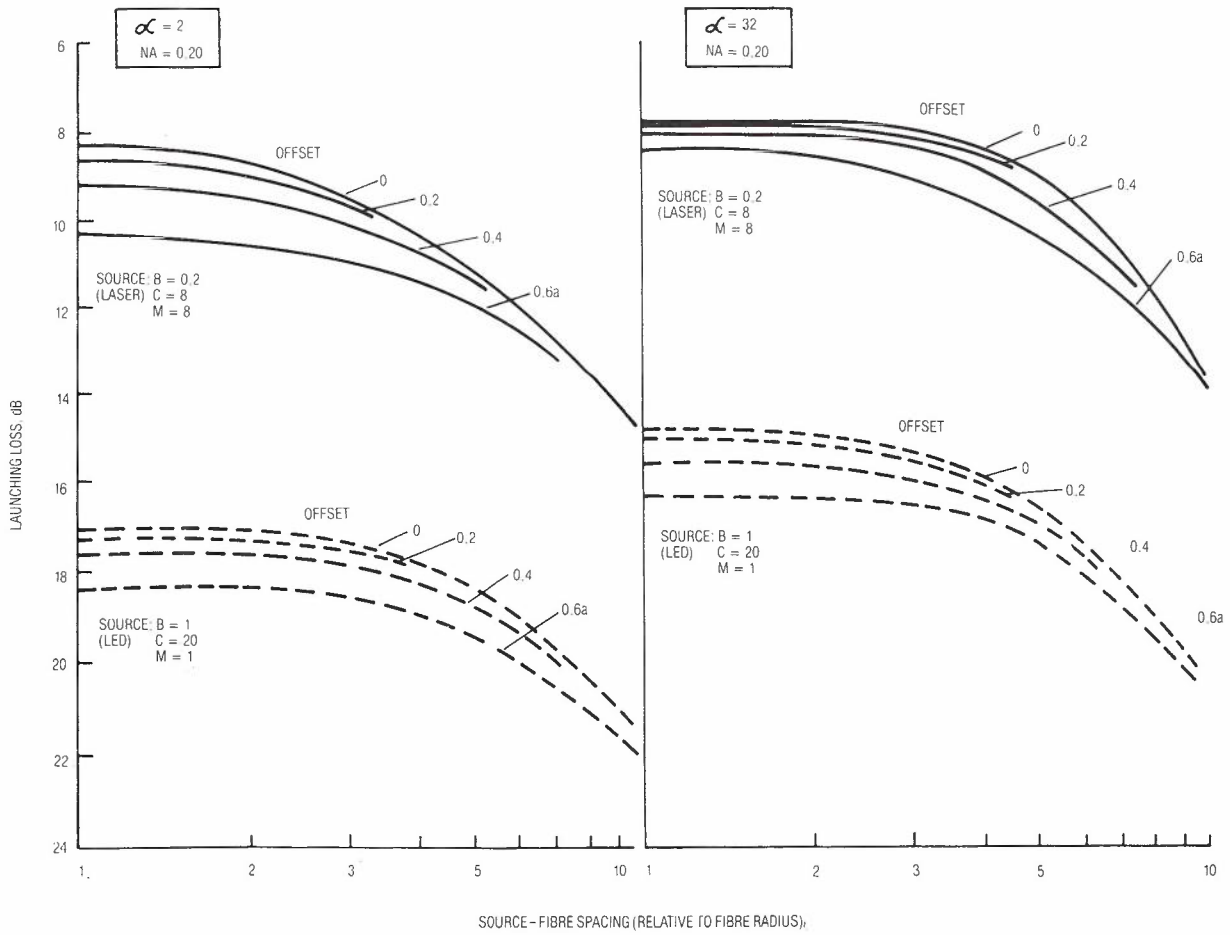

Fig.6 - Launching Losses as a Function of Spacing.

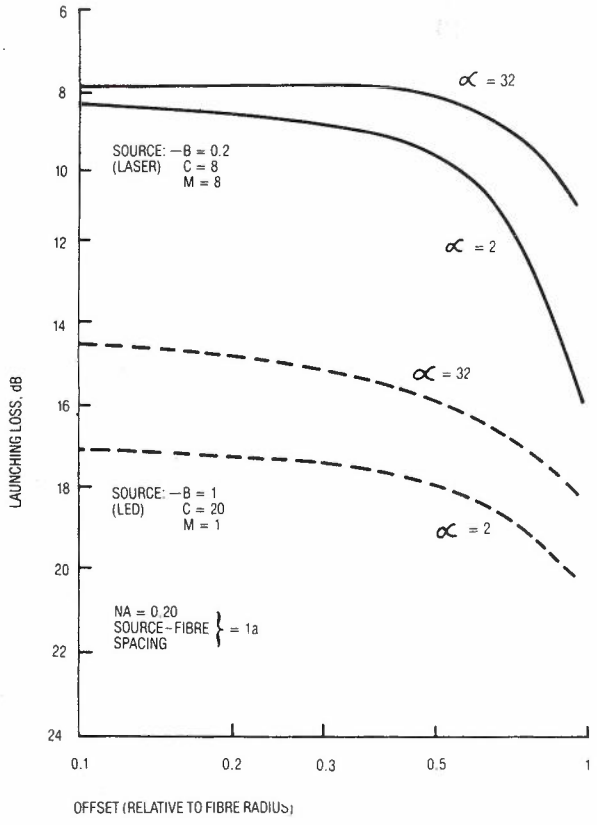

Fig.7 - Launching Losses as a Function of Offset.

Fibre 1 (exciting fibre)

- index profile

$$n_a(\ell) = n_1 \left[1 - \left(\frac{n_1 - n_2}{n_1} \right) \cdot \left(\frac{\ell}{R_1} \right)^{\alpha} \right] , \quad 0 < \ell \leq R_1$$

$$= n_2 , \quad \ell > R_1$$

- near field intensity distribution

$$I(\ell) = \frac{1 - e^{-BC}}{1 - 2e^{-BC} + e^{C(B-\ell)}} , \quad 0 < \ell \leq R_1$$

$$= 0 , \quad \ell > R_1$$

- far field radiation proportional to $\cos^m\phi$.

Fibre 2 (excited fibre)

- index profile

$$n_b(r) = n_1 \left[1 - \left(\frac{n_1 - n_2}{n_1} \right) r^{\alpha} \right] , \quad 0 < r \leq 1$$

$$= n_2 , \quad r > 1$$

The spacing between fibres D, the offset d, Fibre 1 radius R_1 and the effective intensity radius B are all normalised to Fibre 2 radius.

Consider first the total power radiated from an elemental area ds_1 at radius ℓ on the source fibre. Let us assume that the fibre is sufficiently long for all leaky rays to have been attenuated out. The cone into which rays will be radiated is therefore determined by the local numerical aperture at ℓ; ie the half-angle $\phi_c(\ell)$ of this cone is given by

$$\phi_c(\ell) = \sin^{-1} \left[n_a^2(\ell) - n_2^2 \right]^{\frac{1}{2}}$$

If the flux varies as $\cos^m\phi$ as considered earlier to take into account variations in the far field radiation pattern, then the power emitted into the cone from ds_1 is

$$\Delta P = 2\pi \, I(\ell) \int_0^{\phi_c(\ell)} \cos^m\phi \, \sin\phi \, d\phi ds_1$$

$$= \frac{2\pi}{m+1} \, I(\ell) \left[1 - \cos^{m+1}\phi_c(\ell) \right] ds_1$$

The total power emitted from the fibre is then

$$P_{tot} = \frac{4\pi^2}{m+1} \int_0^{R_1} \ell I(\ell) \left(1 - \cos^{m+1}\phi_c(\ell) \right) d\ell \qquad (15)$$

The power launched into Fibre 2 can be calculated in the same way as in the previous section, noting however that in this case $I(\ell)=0$ for $\ell > R_1$. Note also that although the element ds_1 on fibre 1 may lie in the region of excitation for ds_2 on fibre 2 as defined by equation 8, it will not contribute to the power accepted at ds_2 if the angle θ_{za} is greater than the local critical angle $\phi_c(\ell)$ at ℓ on fibre 1.

A long perfect fibre in which all modes are equally excited, and in which leaky modes are

ignored, will have a near field intensity distribution approximating the index profile (Ref 7). On the other hand a fibre that is only partially excited, or in which there is considerable mode-mixing, will have most of its bound energy concentrated towards the centre of the core. It would therefore be anticipated that the effects of coupling mismatches are less significant for this situation than for uniform excitation.

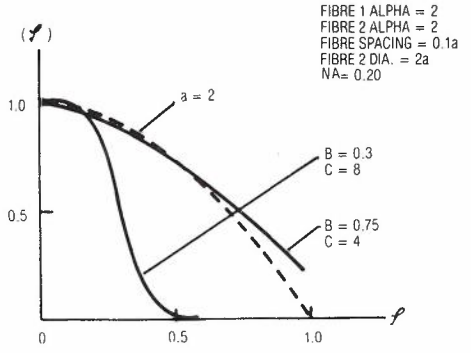

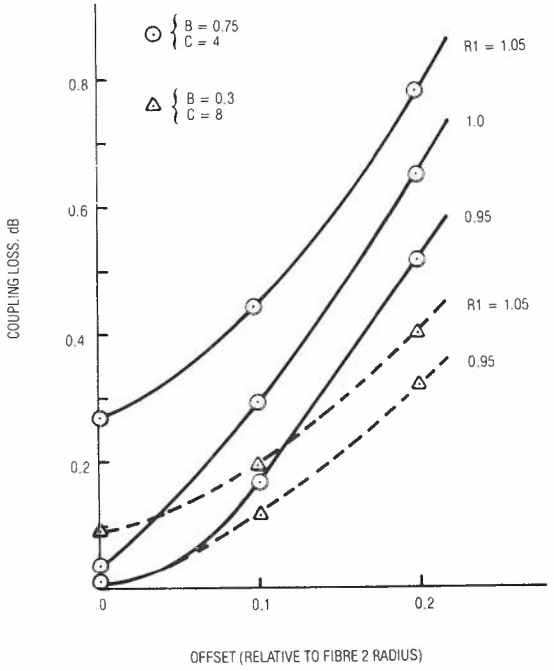

Fig.8 - Coupling Losses as a Function of Offset, Diameter Difference and Excitation Conditions (α = 2).

This anticipated result is demonstrated in Fig 8 for coupling between two fibres having parabolic profiles. Two distributions are assumed for the near field intensity of Fibre 1, the first with B = 0.75 and C = 4 approximates the equal excitation condition, while the second with B = 0.3 and C = 8 represents what might be expected in a practical situation. It is seen that the coupling loss as a function of the axial offset between the fibres is significantly lower for the second intensity distribution. As an example, consider coupling between two fibres with the first having a 5% larger core diameter than the second. If the cladding diameters are twice the core diameters this gives an offset of 10% of the core radius of Fibre 2, assuming that the claddings are aligned at one point. From Fig 8 a coupling loss of 0.45 dB would be predicted under these conditions for uniform excitation, whereas a loss of only 0.2 dB would occur if the actual excitation was of the second form assumed.

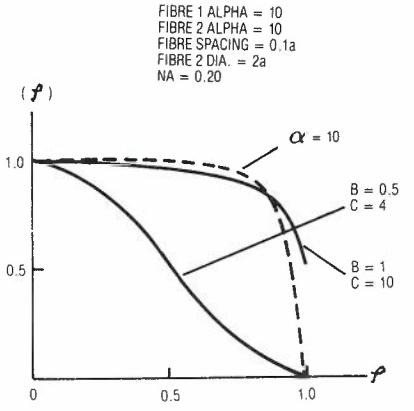

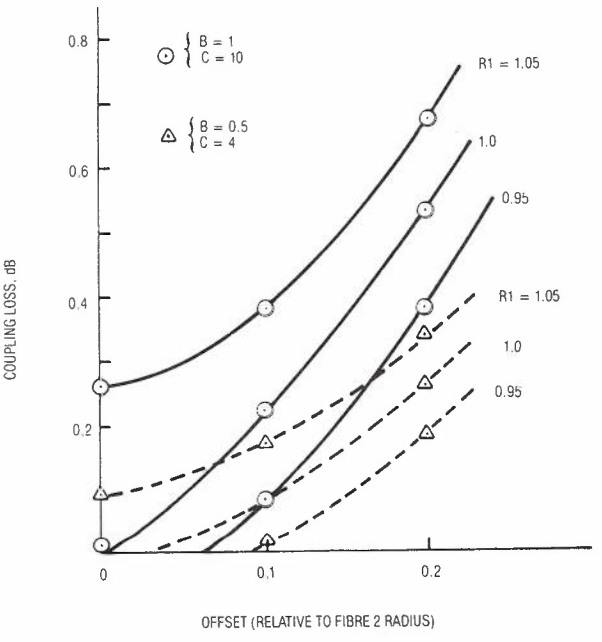

Fig.9 - Coupling Losses as a Function of Offset, Diameter Difference and Excitation Conditions (α = 10).

In Fig 9 similar results are shown for coupling between two fibres having alpha values of 10 (ie tending towards a step-index profile). The condition B = 1, C = 10 corresponds to equal excitation, while the condition B = 0.5, C =4 might represent the near field distribution in a practical situation.

The effects of the spacing between fibres of equal core diameter as a function of offset and excitation conditions are illustrated in Fig 10. It is seen that the influence of fibre offset dominates that of spacing at least for small spacings.

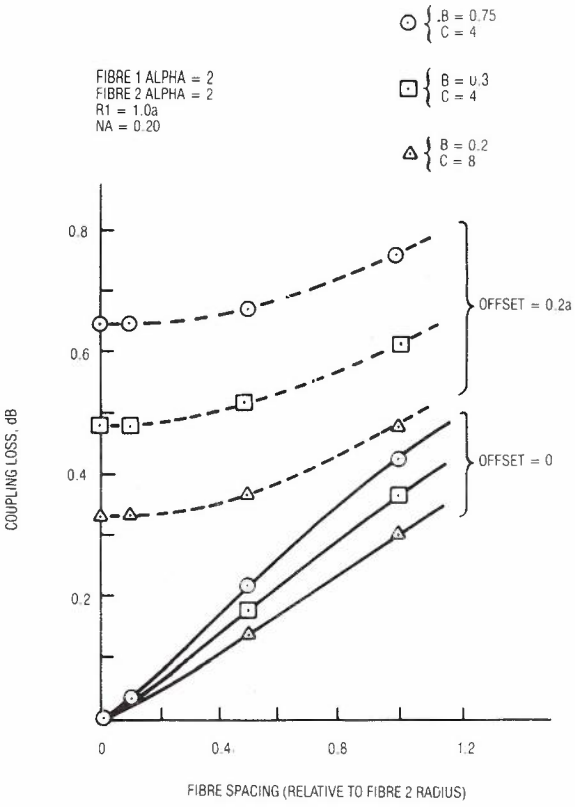

Fig.10 - Coupling Losses as a Function of Fibre Spacing, Offset and Excitation Conditions (α = 2).

4. CONCLUSION

A method for calculating launching and coupling efficiencies between source and fibre or between fibres based on a straightforward geometrical analysis has been described. Using this approach it is possible to assess the individual or combined effects of arbitrary variations in most of the source and fibre parameters likely to occur in practical coupling situations. It has been demonstrated, for example, that for a near field power distribution concentrated towards the centre of the fibre (as might be expected due to mode mixing or partial excitation) the coupling losses can be less than half the value (in dB) which would result if all modes were equally excited. Further the effects of diameter variations at joints is significantly less for this form of intensity distribution.

Another interesting result suggests that the coupling efficiency between a stripe geometry injection laser (of the dimensions likely to be used in fibre systems) and an arbitrary profile fibre may be able to be calculated sufficiently accurately by assuming a symmetrical source having the near-field characteristics appropriate to the plane of the junction and the far-field characteristics appropriate to a plane perpendicular to the junction.

5. REFERENCES

1. Di Vita, P. and Vannucci, R., "Geometrical Theory of Coupling Errors in Dielectric Optical Waveguide", Optics Communications, Vol.14, No.1, May 1975, pp 139-144.

2. Di Vita, P. and Vannucci R., "Multimode Optical Waveguides with Graded Refractive Index : Theory of Power Launching", Applied Optics Vol.15, No.11, Nov 1976, pp 2765-2772.

3. Marcuse, D., "Excitation of Parabolic-index Fibres with Incoherent Sources", Bell Syst Tech J., Vol.54, No.9, Nov 1975, pp 1507-1530.

4. Gloge, D., "Offset and Tilt Loss in Optical Fibre Splices", Bell Syst Tech J., Vol.55, No.7, Sept 1976, pp 905-916.

5. Thiel, F. and Hawk, R., "Optical Waveguide Cable Connection", Applied Optics Vol.15, No.11, Nov 1976, pp 2785-2791.

6. Longhurst, R.S., "Geometrical and Physical Optics", 1967 (Longman).

7. Adams, M., Payne, D., and Sladen, F. "Leaky Rays on Optical Fibres of Arbitrary (circularly symmetric) Index Profiles", Elec Letts Vol.11, No.11, 29 May 1975,pp 238-240.

8. Benson, W., Pinnow, D., and Rich, T., "Coupling Efficiency Between GaAlAs Laser and Low Loss Optical Fibres". App Optics Vol.14, No.12, Dec 1975, pp 2815-2816.

9. Miller, C., "Transmission vs Transverse Offset for Parabolic-profile Fibre Splices with Unequal Core Diameters", Bell Syst Tech J., Vol.55, No.7, Sept 1976, pp 917-927.

BIOGRAPHY

GRAEME P. KIDD obtained his Engineering degree at the University of Queensland in 1961 and his science degree at Melbourne in 1965. He joined the A.P.O. Research Laboratories in 1962. In 1968 he became Divisional Engineer of the Transmission Lines Division which subsequently became the present Guided Media Section. He has been concerned with the characteristics of high-capacity circular waveguide, and was seconded to the B.P.O. Research Department in 1970-71 to study developments in this area. Since 1972 his main interest has been with optical fibres.

Transient Events in Phase-Locked Loops

J. L. PARK
Telecom Australia Research Laboratories

In order to make the best use of phase-locked loops it is important to have a design oriented understanding of them. This paper investigates the validity of a piecewise-linearized model of the phase-locked loop with a sinusoidal phase comparator. The model under consideration was proposed by Badcock to enable investigation of the performance of the phase-locked loop near threshold.

Results of practical measurements of loss-of-lock rates are given and compared with those predicted by the model. It is shown that by appropriate methods of analysis the model can yield acceptable loss-of-lock rate predictions over a wide range of input signal-to-noise ratio and loop bandwidth.

1. INTRODUCTION

The exact analysis of the response of a phase-locked loop to a noisy signal has been achieved only for a limited case: a loop with no filtering and an unmodulated carrier plus white noise input. Practical loops generally incorporate loop filters and are often preceded by band-pass filters. The difficulties of analysis can be attributed to the combination of an instantaneous non-linearity and energy-storage elements in the feedback loop. An extensive list of references has been provided by Badcock (Ref.1).

Equations can be written describing the operation of the phase-locked loop, but in general these equations have evaded solution. The nature of the solution is fairly well understood. The differences between loops of varying complexity are mainly quantitative, rather than qualitative. Second order phase-locked loops are most widely used in practice while higher-order loops are less widely used. Quite a number of approximate results have been obtained for second-order loops.

Badcock (Ref.1) proposed a piecewise-linear approximation of the nonlinear element in the phase-locked loop. He split the operation of the phase-locked loop up into four regions and then analysed it in the various regions using the results from one region to obtain boundary conditions for the next. Badcock was able to produce theoretical curves of the expected loss-of-lock rate of the voltage-controlled oscillator (VCO) in the loop with respect to the input signal for various bandwidths of input noise.

In performing his calculations, Badcock made several assumptions regarding the spectra of the noise components, the possibility of multiple loss-of-lock and the conditions necessary during a transient event for loss-of-lock to occur.

This paper presents the results of an investigation leading to improvements in the proposed model of the phase-locked loop. Practical measurements of loss-of-lock rates were obtained for various loop bandwidths and are compared with those estimated using the original and improved models.

2. BADCOCK'S MODEL

Badcock considered a phase-locked loop as shown in Fig 1. The phase comparator was assumed to contribute a sinusoidal non-linearity. In order to facilitate the treatment of noise in the phase-locked loop, it is desirable that the non-linear element be linearized. However, it can be shown that a single linear approximation is not satisfactory for investigations of the loop operation near threshold since it is based on the very assumptions which are violated near threshold, i.e. of high signal-to-noise ratio and linear operation of the loop.

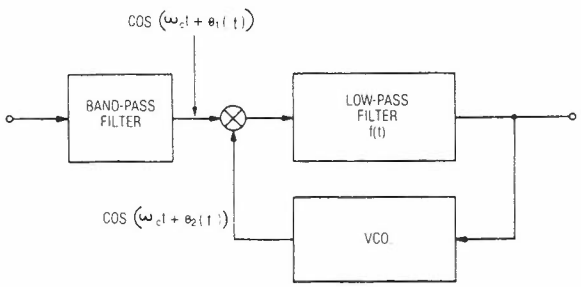

Fig.1 - Phase-locked Loop.

In the piecewise-linear model the range $-\frac{\pi}{4} \leq \theta \leq 7\frac{\pi}{4}$, where θ is the phase difference between the VCO and input signals, (with phases of θ_2 and θ_1, respectively), is broken up into four regions, in which the following approximations are made for the sinusoidal non-linearity.

Region	Range of θ (radians)	Approximation for sin θ
1	$-\frac{\pi}{4} < \theta \leq \frac{\pi}{4}$	θ
2	$\frac{\pi}{4} < \theta \leq \frac{3\pi}{4}$	1
3	$\frac{3\pi}{4} < \theta \leq \frac{5\pi}{4}$	$\pi - \theta$
4	$\frac{5\pi}{4} < \theta \leq \frac{7\pi}{4}$	-1

This is illustrated in Fig 2.

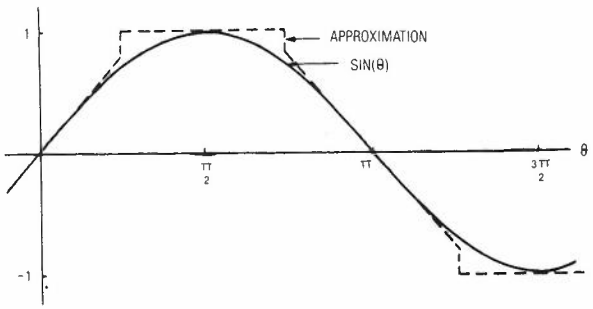

Fig.2 - Approximation to sin(θ).

When θ is outside the range $\frac{-\pi}{4}$ to $\frac{7\pi}{4}$ radians it is brought within the range by adding or subtracting integral multiples of 2π radians. When θ lies in region 1, the model is said to be in state 1, and so on.

Badcock investigated the response of the piecewise-linear model to a noisy input. He resolved the input noise into components in-phase and in-quadrature with the VCO waveform, this being a convenient reference. He then used the spectral densities of the resolved components and the differential equations for the piecewise-linear model to find the variance of the VCO phase, $\theta_2(t)$, in region 1 ($\frac{-\pi}{4} < \theta < \frac{\pi}{4}$ radians). Hence the frequency of transitions to region 2 was found, assuming region 1 to be the normal, or equilibrium state.

The piecewise-linear model was then analysed in region 2, ($\frac{\pi}{4} < \theta < \frac{3\pi}{4}$ radians). It was assumed that if $\theta(t)$ entered region 3, ($\frac{3\pi}{4} < \theta < \frac{5\pi}{4}$ radians) then loss-of-lock would occur. Hence the expected loss-of-lock rate was calculated.

It was found necessary to assume some form of pre-loop filtering in order to make the analysis possible. This does not imply that pre-loop filtering is necessary in the physical phase-locked loop. In any case, some form of pre-loop filtering is generally used to restrict the range of the phase comparator.

2.1 Assumptions Associated with the Piecewise-linear Model

(i) It was assumed that the spectra of the input noise as resolved into quadrature components with respect to the VCO waveform were of the same shape as the components of the input noise as resolved with respect to the input carrier waveform. However, the VCO is not of fixed frequency - it responds to some extent to the resultant of the input carrier and added input noise. Hence the spectra will not be as assumed.

(ii) It was assumed that when $\theta(t)$ entered region 3, that is, became greater than $\frac{3\pi}{4}$, a loss-of-lock event would inevitably occur. This assumption is invalid. $\theta(t)$ can, in fact, enter some distance into region 3 and still not result in loss-of-lock.

(iii) It was assumed that multiple loss-of-lock events would not be signigicant.

3. RESOLVED COMPONENTS OF THE INPUT NOISE

3.1 Outline

In order to improve Badcock's analysis of the piece-wise-linear phase-locked loop, it is necessary to obtain information about the components of the input noise as resolved with respect to the VCO waveform. The spectra of these components are a starting point in the analysis and, as will be shown, can have a substantial effect on the expected loss-of-lock rate. An exact analysis of these spectra is not available since this would involve an exact solution for the dynamics of the phase-locked loop which has not, as has previously been noted, been performed to date.

A possible method of analysis is to use the linear model of the phase-locked loop to calculate the spectra of the resolved components. To these spectra it would then be necessary to add a component to account for the presence of loss-of-lock events. Rice (Ref 2) has used a similar procedure for this type of analysis. Such calculations are very difficult without specifying particular forms for the input noise and loop characteristics.

3.2 Heuristic Treatment of the Noise Components

An intuitive idea of the shape of the spectra can be obtained by considering the physical behaviour of the phase-locked loop. Let us define the "loop bandwidth" as the equivalent rectangular bandwidth of the linearized system.

Further, let us define the "input signal-to-noise ratio" as the signal-to-noise ratio measured after the pre-loop filter but before the input to the phase-locked loop. The total input signal to the phase-locked loop is the resultant of the input noise and the carrier. The feedback mechanism of the phase-locked loop attempts to

phase-lock the VCO and input signals. The speed of response of the phase-locked loop is limited since the loop transfer function $\theta_2(S)/\theta_1(S)$ is low-pass. Hence, the VCO can follow the low frequency components of the noise (as compared with the input carrier frequency) more easily than the high frequency components.

Consider the input noise as resolved into components in-phase, $p_1(t)$, and in-quadrature, $q_1(t)$, with the VCO waveform. Since the VCO is able to follow the low frequency components of the input noise more easily than the high frequency components, the low frequency content of $p_1(t)$ and $q_1(t)$ will be less than for the components, $p(t)$ and $q(t)$, resolved with respect to the input carrier frequency. This may be summarized as follows:

(i) If $Wq(\omega)$, the spectrum of the input noise as resolved with respect to the input carrier, is very broad compared with $G(\omega)$, the loop bandwidth, then the VCO phase will not vary significantly in response to the noise and $Wq_1(\omega)$ will be similar to $Wq(\omega)$.

(ii) If $Wq(\omega)$ is very narrow compared with $G(\omega)$, the VCO phase will vary due to the noise over the whole bandwidth of $Wq(\omega)$. Hence, $Wq_1(\omega)$ will have shape and bandwidth similar to $Wq(\omega)$ but of reduced magnitude.

(iii) For cases intermediate between (i) and (ii) above, a significant amount of power will be removed from the lower frequency portion of $Wq(\omega)$ to give $Wq_1(\omega)$ but substantially less than from the high frequency portion. Hence $Wq_1(\omega)$ will have a broader spectrum than $Wq(\omega)$.

(iv) Loss-of-lock events contribute to further widening of the spectrum since, being basically impulsive events, they add a white component to the noise. The widening will be most pronounced when the input bandwidth is small compared with the loop bandwidth, given a constant total noise power, since the number of loss-of-lock events is greatest under this condition.

3.3 Experimental Measurement of the Power Spectral Densities of $p_1(t)$ and $q_1(t)$

Representative, as distinct from comprehensive, results were sought. Obtaining comprehensive sets of results would involve varying each parameter, in succession, through its full range. This would be very time consuming and tedious due to the large number of parameters involved. With this in mind, results were sought near threshold, an area of major interest, and at several higher values of signal-to-noise ratio.

Figures 3, 4, 5, 6 and 7 show the measured spectra of the components of the input noise $p_1(t)$ and $q_1(t)$ for various values of R, the ratio of pre-loop filter equivalent low-pass bandwidth to phase-locked loop equivalent low-pass bandwidth. The curves are plotted for various values of the signal-to-noise ratio measured after the pre-loop filter.

The plots have been magnitude scaled by dividing by the magnitude when resolved with respect to the carrier waveform. The filter bandwidths have been normalized to 1. These plots show the portions of the spectra attenuated by the resolution with respect to the VCO waveform compared with a resolution with respect to the input carrier waveform.

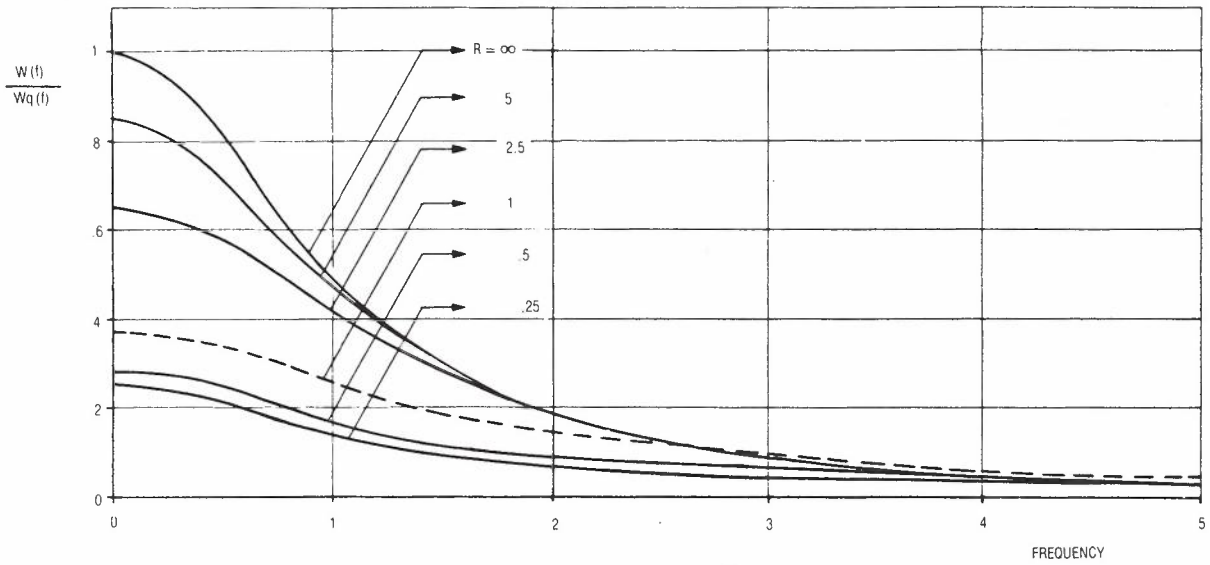

Fig.3 - Spectra of $W_{q_1}(f)$ S/N = -3dB.

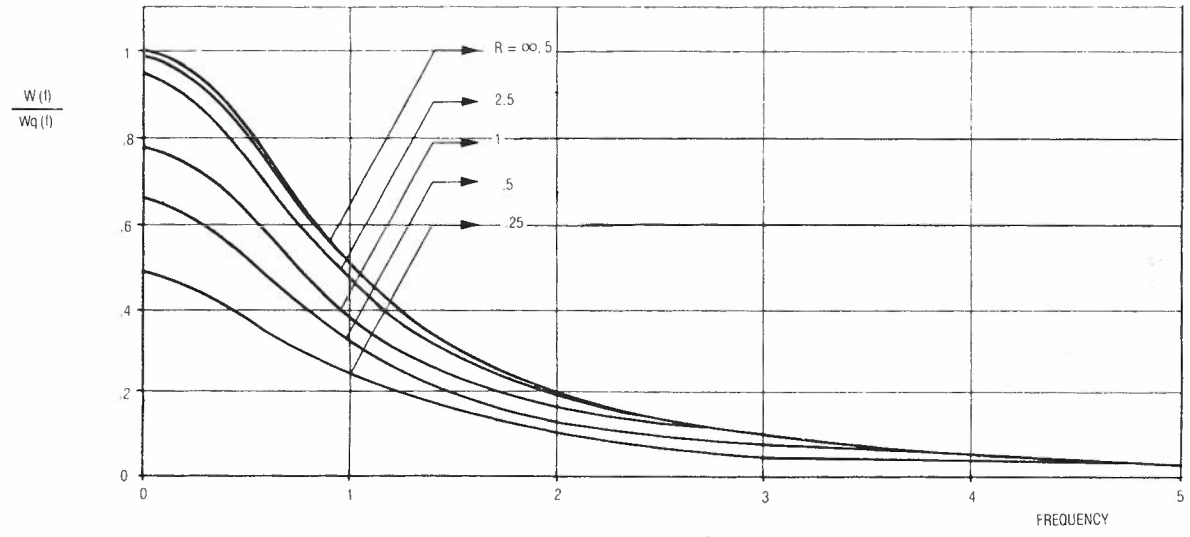

Fig.4 - Spectra of $W_{q_1}(f)$ S/N = +1dB.

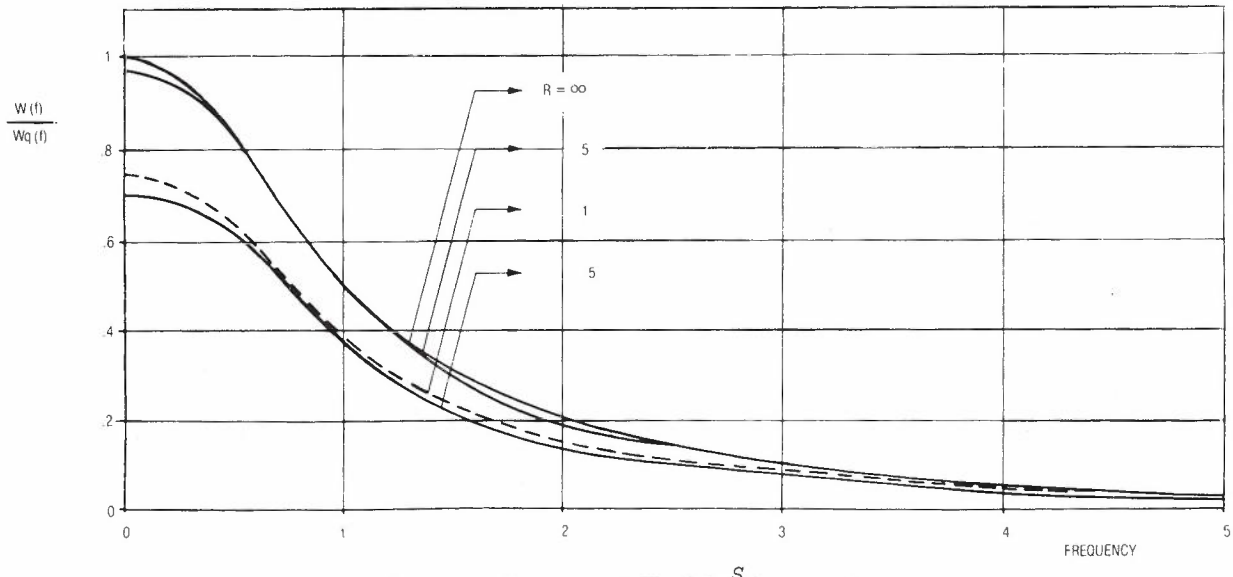

Fig.5 - Spectra of $W_{q_1}(f)$ S/N = +7dB

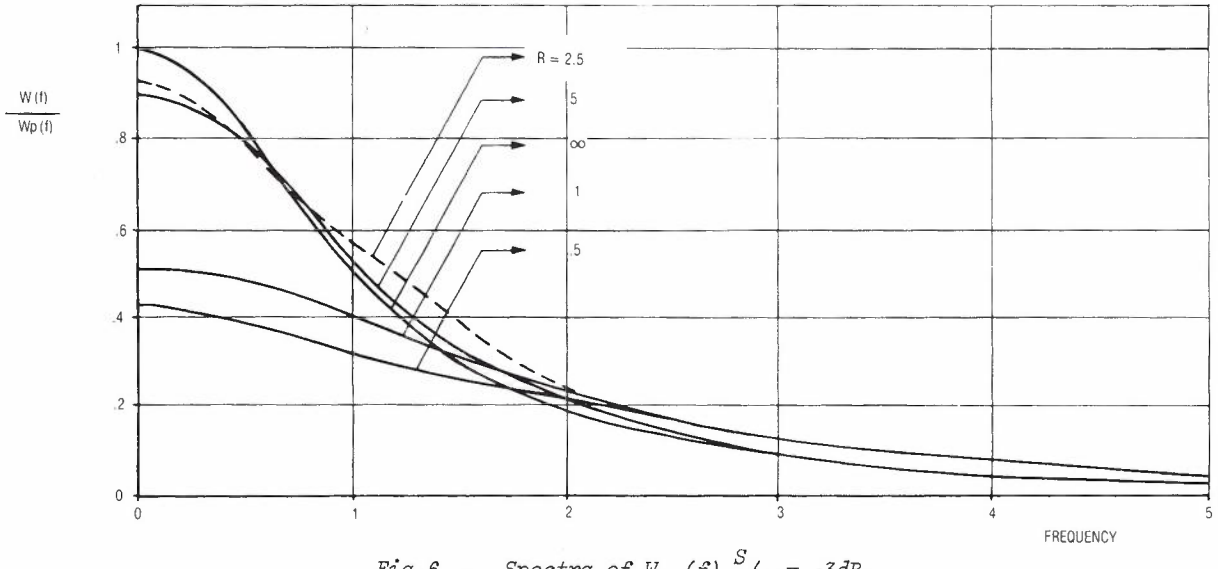

Fig.6 - Spectra of $W_{p_1}(f)$ S/N = -3dB.

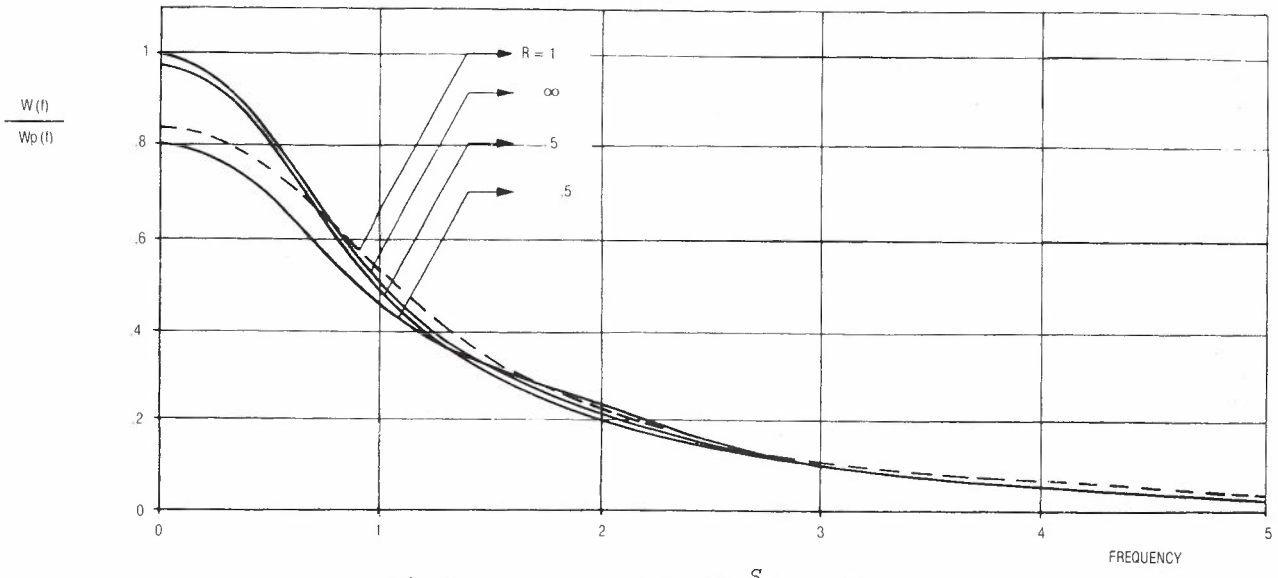

Fig.7 - Spectra of $W_{p_1}(f)$ $S/N = +7dB$.

Figure 8 gives a plot of points from Figs.3 to 7 for zero frequency. This enables an easy comparison of the attenuation at this frequency.

It can be seen that if R is greater than 1 and increases, then the spectra $Wp_1(\omega)$ and $Wq_1(\omega)$ become more similar to $Wp(\omega)$ and $Wq(\omega)$, both in magnitude and shape. Also, it can be seen that if R is less than 1 and decreases, the shape of the spectra $Wp_1(\omega)$ and $Wq_1(\omega)$ become similar to that of $Wp(\omega)$ and $Wq(\omega)$ but of reduced magnitude. When R is of the order of 1 the spectra $Wp_1(\omega)$ and $Wq_1(\omega)$ are seen to be broader than $Wp(\omega)$ and $Wq(\omega)$. $Wp_1(\omega)$ and $Wq_1(\omega)$ are seen to have significantly less power in the low frequency area than $Wp(\omega)$ and $Wq(\omega)$.

The contribution to the spectra from loss-of-lock events can be seen from Figs.3 and 6. It can be seen that for R < 1 the tails of the spectra are of a greater magnitude than expected in the absence of loss-of-lock events. They are of the form which would be obtained upon adding a component of wideband noise, such as loss-of-lock events. It can be seen, particularly from Fig.8, that the magnitudes of $Wp_1(\omega)$ and $Wq_1(\omega)$ are much closer to the magnitudes of $Wp(\omega)$ and $Wq(\omega)$ for higher signal-to-noise ratios.

Generally, the results are as predicted previously.

4. ANALYSIS OF THE PHASE-LOCKED LOOP PIECEWISE-LINEAR MODEL

The analysis of the piecewise-linear model of the phase-locked loop by Badcock (Ref.1) may be extended using the actual spectra of $p_1(t)$ and $q_1(t)$. To this end, it is of value to outline the calculations performed in this analysis.

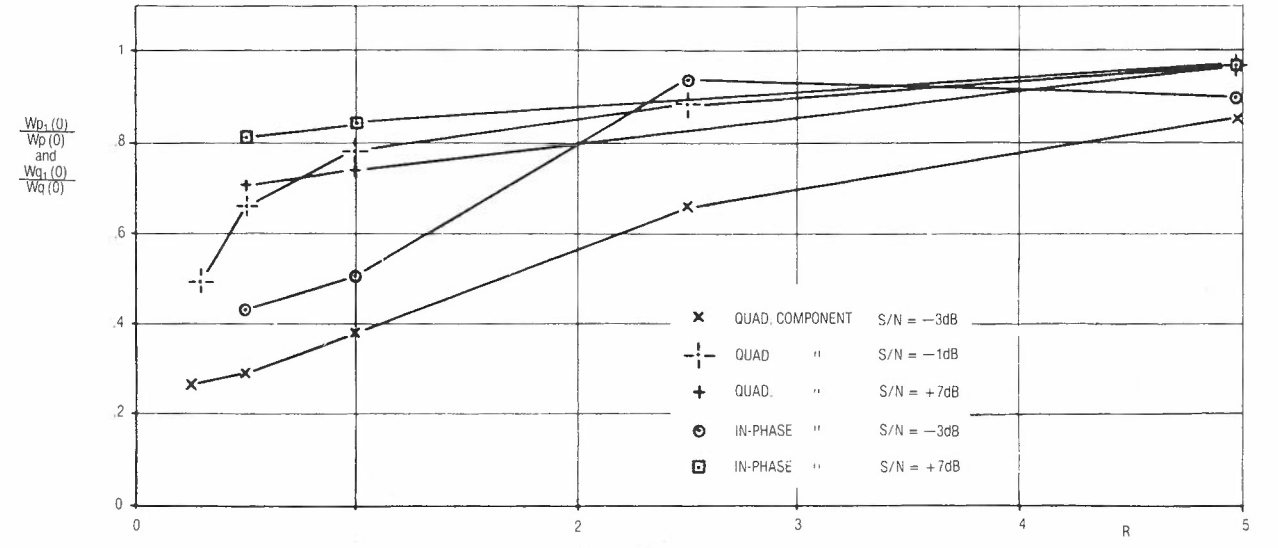

Fig.8 $\frac{W_{p_1}(0)}{W_p(0)}$ *AND* $\frac{W_{q_1}(0)}{W_q(0)}$

It can be shown (Ref.3) pp.426-8 or (Ref.4) p.193, that the expected number of upwards crossings per second of a level μ_o by a stationary random gaussian process u(t), of zero mean and one-sided power spectral density Wu(ω) is

$$E(u) = \frac{1}{2\pi}\sqrt{\frac{b_2}{b_o}} \cdot \exp\left(\frac{-u_o^2}{2b_o}\right) \qquad (1)$$

where

$$b_o = \int_o^\infty W_u(\omega)d\omega \qquad (2)$$

and

$$b_2 = \int_o^\infty \omega^2 W_u(\omega)d\omega \qquad (3)$$

b_o can be seen to be the variance of u(t) and b_2 the variance of the derivative of u(t).

The frequency and velocity with which the VCO phase $\theta_2(t)$ exceeds $\frac{\pi}{4}$ radians is required for the phase-locked loop model.

In state 1 of the model the one sided spectral density of $\theta_2(t)$ is, for a second-order loop:

$$W_{\theta_2}(\omega) = \frac{1 + \omega^2\tau^2}{1 + \frac{2\omega^2}{\omega_n^2}(\omega^2\zeta^2 - 1) + \frac{\omega^4}{\omega_n^4}} \cdot \frac{W_{q_1}(\omega)}{A^2} \qquad (4)$$

where A = input signal level

ζ = loop damping factor

τ = time constant of the loop zero.

ω_n = natural frequency (radians).

It is evident from this equation that b_2, (equation 3), will not be finite unless $Wq_1(\omega)$ is low-pass at least to the extent of being shaped by a single pole.

Once the model has entered state 2 the question is whether it leaves by entering state 3 or returning to state 1.

In state 2, the model is described by

$$\frac{\tau}{K} \cdot \frac{d^2\theta_2}{dt^2} = -1 + \frac{q_1}{A} + \frac{\tau}{A} \cdot \frac{dq_1}{dt} \qquad (5)$$

where K = gain constant of the loop.

The solution of equation (5) contains a deterministic component and a Gaussian random, non-stationary, component. Although the velocity of entry into region 2, $\left.\frac{d\theta_2}{dt}\right|_{\text{upon entry}}$, is random, it is convenient to include this in the deterministic component because it is a boundary condition whose probability distribution is a consequence of state 1 bahaviour.

Taking the time origin at the instant of entry, the deterministic component is

$$\theta_{2d}(t) = \frac{-Kt^2}{2\tau} + \omega_o t + \frac{\pi}{4} \qquad (6)$$

Because the initial velocity has been included here, the initial velocity of the random component (as well as the initial value) must be zero. Badcock investigated various non-stationary processes and obtained the covariance function of the random process arising from the last two terms of equation (5), where $q_1(t)$ was assumed to arise from single-pole filtering of white Gaussian noise and the initial slope was constrained to zero.

It can be shown (Ref.1),(pp 207-218) that the probability of an upwards exit can be looked upon as the consequence of an artificial Gaussian random error in ω_o, the remainder of the trajectory being assumed to be deterministic. That is, assume the initial velocity is

$$\omega = \omega_o + \gamma \qquad (7)$$

where γ is Gaussian with zero mean and a variance of σ_γ. The peak of a deterministic trajectory with some given value of ω is

$$\theta_{2\,max} = \frac{\pi}{4} + \frac{\omega^2}{2} \qquad (8)$$

which must be greater than $\frac{3\pi}{4}$ for an upwards exit to occur. Thus the probability of upwards exit given ω_o is

$$P\left[\frac{\omega^2}{2} > \frac{\pi}{2}\right] = \int_{-\infty}^{\omega_o - \sqrt{\pi}} \frac{1}{\sqrt{2\pi\sigma_\gamma}} \cdot \exp\left(\frac{-\gamma^2}{2\sigma_\gamma^2}\right) d\gamma \qquad (9)$$

The problem is to find the value of σ_γ for any particular set of loop parameters. This can

be fairly easily done for any likely form of loop filter using the covariance function of the random process arising from the last two terms of equation (5) (Ref.1, pp.220-225).

The expected number of entries into region 2 from region 1, the probability density for the velocity of entry and the probability of upwards exit from region 2 for any ω_o can now be combined to give the expected number of entries into region 3.

Assuming that each entry into region 3 results in a loss-of-lock event, and allowing for clockwise as well as anticlockwise phase rotations, the expected number of loss-of-lock events per second is:

$$\bar{N} = \frac{1}{\pi^2 \sqrt{b_o}\sigma_\gamma} \cdot \exp\left[-\frac{\left(\frac{\pi}{4}\right)^2}{2b_o}\right] \cdot \int_0^\infty \exp\left(\frac{-\omega_o^2}{2b_2}\right) \int_{-\infty}^{\omega_o - \sqrt{\pi}} \exp\left(\frac{-u^2}{2\sigma_\gamma^2}\right) du\, d\omega_o \qquad (10)$$

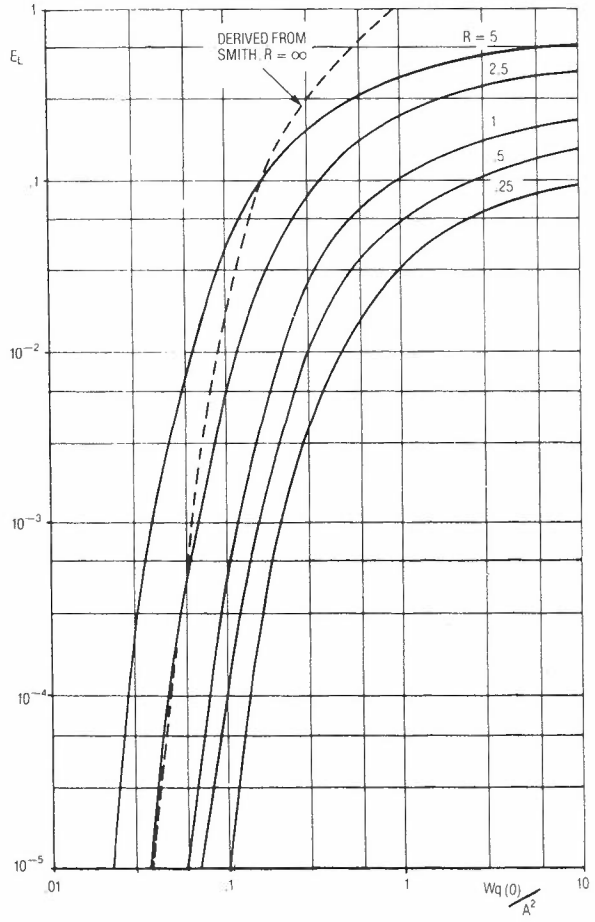

Fig.9 - Expected frequency of loss-of-lock events. Calculated results using $W_q(f)$.

Figure 9 gives plots of the expected frequency of loss-of-lock events for various bandwidths of the pre-loop filter and various values of $\frac{Wq_1(o)}{A^2}$, (the magnitude of the resolved component of noise at zero frequency). These plots were derived using equation (10). A curve derived from Smith (Ref.5) and modified by Badcock is also shown, for comparison.

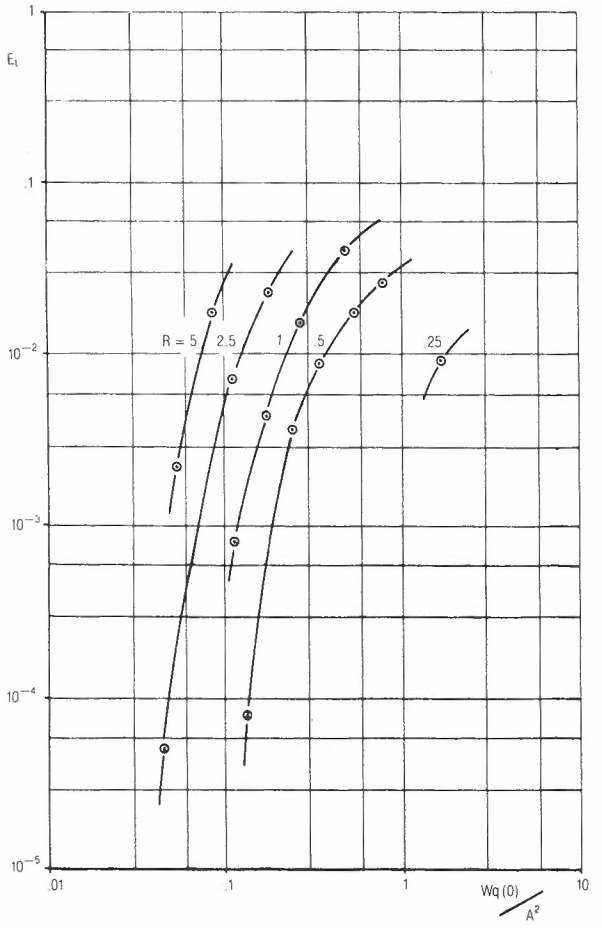

Fig.10 - Expected frequency of loss-of-lock events - measured results.

Figure 10 gives plots of the measured loss-of-lock rate from the experimental model used in the investigations.

Comparing the predicted results using Badcock's model and the measured results it can be seen that the results predicted are pessimistic. For large values of R, say R>5, the predicted and measured results are in good agreement. As R decreases the measured results become an increasingly smaller proportion of the predicted results. The extent of the discrepancy is, however, not so large as to render the model unworkable.

5. USE OF THE SPECTRA OF $p_1(t)$ AND $q_1(t)$

It was shown in section 3 that the spectrum of $q_1(t)$ may be quite different from that of

q(t). This section is concerned with the improvement in accuracy of the predicted loss-of-lock rate available by using the actual spectrum of $q_1(t)$ in Badcock's model.

The parameters of $q_1(t)$ used in the initial calculations were $Wq_1(o)$ and the half power bandwidth, assuming that the spectra were shaped by a single pole. The parameters of $Wq_1(\omega)$ were taken to be identical to those of $Wq(\omega)$ which were known.

A simple improvement for the calculation of expected loss-of-lock rate is to use the measured values of $Wq_1(o)$ and half power bandwidth, still assuming shaping by a single pole. Figure 11 gives plots of the expected loss-of-lock rate using this technique. Comparing these results with those measured and those calculated using Badcock's method it can be seen that:

(i) The expected loss-of-lock rates from all these methods are very similar for R>>1.

(ii) For R<<1 the predictions using the measured parameters of $q_1(t)$ are in good agreement with those measured. Both these rates are substantially different from predictions using Badcock's method.

(iii) For R≈1 the expected loss-of-lock rates using either method of prediction are in error by a significant amount.

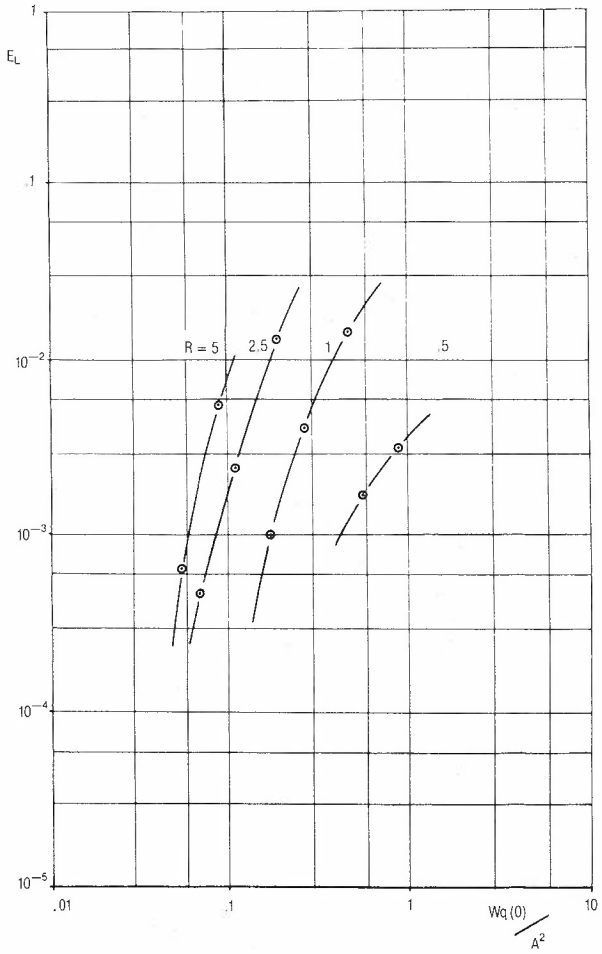

Fig.11 - Expected frequency of loss-of-lock events - calculated results using $W_{q_1}(f)$.

As shown in section 3, the shape of the spectrum of $q_1(t)$ is very similar to that of q(t) for R>>1 or R<<1 but markedly different for R≈1. Consequently the single pole representation for the spectrum of $q_1(t)$ is not sufficiently accurate for R≈1.

A method for improving the estimate of loss-of-lock rate using the measured values of $Wq_1(\omega)$ is as follows:

(i) Graphically integrate the difference between the plot of $Wq_1(\omega)$ and the plot for a single pole roll-off filter.

(ii) Subtract this area from the equivalent rectangular filter for the single pole case.

(iii) Hence, obtain the equivalent rectangular filter for $Wq_1(\omega)$, having the same value at $\omega = o$ and the same area.

(iv) Obtain the equivalent bandwidth of the single pole filter of best fit.

(v) Apply these parameters to equation 10 to obtain an estimate of the loss-of-lock rate.

Results of such calculations are given in Table 1

TABLE 1 - Loss-of-lock Rate.

R	$\frac{W_q(o)}{A^2}$	Calculated loss-of-lock rate	Measured loss-of-lock rate
1	.395	.025	.03
1	.157	.0034	.003
1	.0394	3.4×10^{-8}	$\simeq 3 \times 10^{-8}$
.5	.79	.02	.025
.5	.314	.009	.008
.5	.079	7×10^{-6}	$\simeq 10^{-6}$

5.1 Comparison of Predicted and Measured Loss-of-Lock Rates

It can be seen that the calculated and measured loss-of-lock rates are in good agreement and warrant the use of this method when R≈1.

Objections to this method are:

(a) Knowledge of $Wq_1(\omega)$ is needed.

(b) Effects of multiple loss-of-lock and region 3 behaviour have been neglected in the analysis.

It should be noted that it has been assumed that if θ should pass through region 3 into region 4 then a loss-of-lock event does occur. This assumption was tested experimentally by measuring the number of times θ entered region 4 and then returned to region 1 via region 3. The results, although not extensive, indicated that the expected frequency of these transient events was at least two orders of magnitude lower than for complete rotations. Hence the assumption is valid.

6. REGION 3 BEHAVIOUR AND MULTIPLE LOSS-OF-LOCK

Experimental results of the probability of region 4 exit, given entry into region 3, are plotted in Fig.12.

These results show that the probability of region 4 exit given entry into region 3 is relatively constant as R and $\frac{Wq(o)}{A^2}$ change. This would possibly justify assuming that a simple multiplying factor may be used to allow for region 3 behaviour.

It was assumed in the previous analysis that multiple loss-of-lock did not occur. Multiple loss-of-lock can occur when the rate of change of $\theta_2(t)$ after a loss-of-lock event is such that the loop feedback system has insufficient time to reduce this rate of change to zero before $\theta_2(t)$ exceeds π radians.

Figure 13 shows plots of the experimentally measured multiple loss-of-lock rate. A multiple loss-of-lock event is defined as a loss-of-lock event occurring within a time interval,

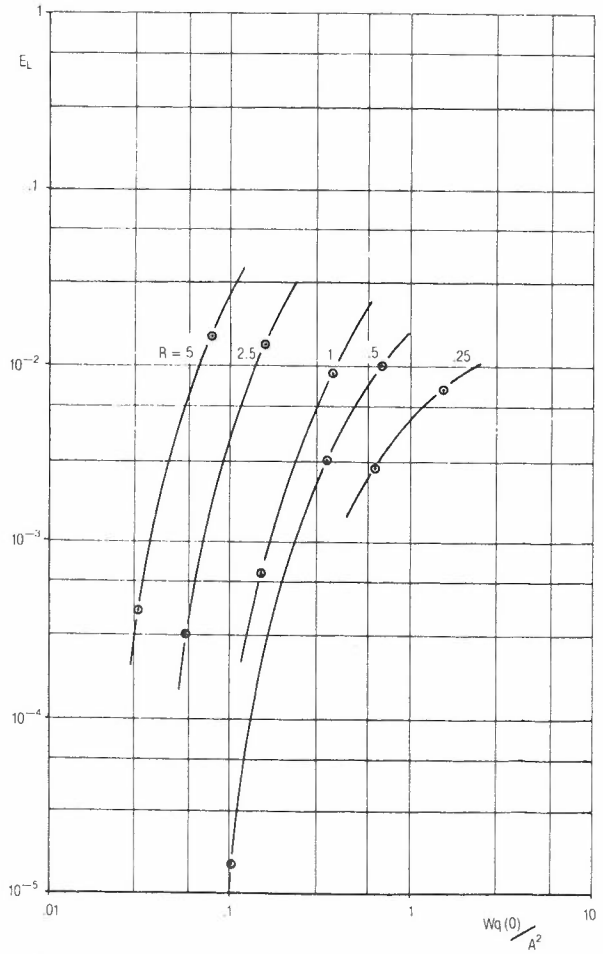

Fig.13 - Expected frequency of loss-of-lock events - multiple events.

Δt = 1/loop bandwidth, of a previous loss-of-lock event as per Ridgway (Ref.6).

The plots, although not extensive, indicate that the number of multiple loss-of-lock events follow the same trends as for single events. It

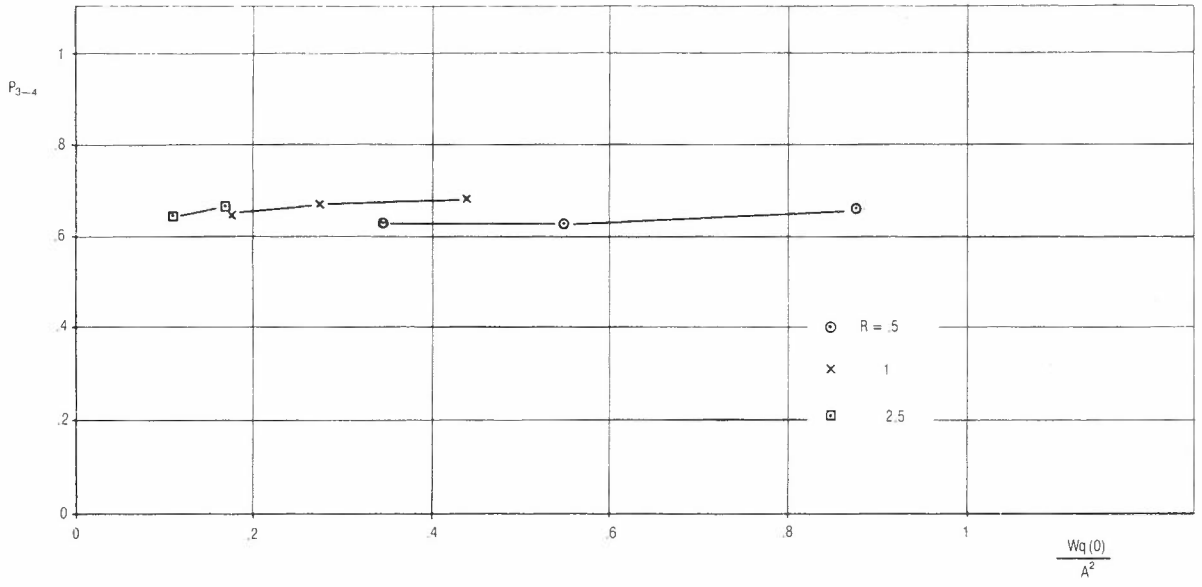

Fig.12 - Probability of region 4 exit given region 3 entry - measured results.

can be seen that the ratio of multiple events to total events is of the order of 0.3.

It can be seen that treating both the effects of region 3 behaviour and multiple loss-of-lock as constant multiplicative factors results in the effects of these factors very nearly cancelling for the cases under investigation.

7. CONCLUSION

It has been found that the piecewise-linear model for the phase-locked loop proposed by Badcock can yield acceptably accurate predictions of loss-of-lock rate if allowance is made for the shape and magnitude of the noise spectra used in the calculations.

It has been shown that the model can be considered in three parts:

(a) The input bandwidth much greater than the loop bandwidth.

(b) The input bandwidth much less than the loop bandwidth.

(c) The input and loop bandwidth comparable.

For (a), the assumption, that the noise as resolved with respect to the VCO has the same spectrum as when resolved with respect to the input waveform, is satisfactory and yields accurate predictions of the loss-of-lock rate. This assumption is not satisfactory for (b) and (c) since the discrepancy between predicted and measured results is too great.

For (b) and (c) it has been shown that using the spectra of the noise as resolved with respect to the VCO, instead of with respect to the input carrier, can yield accurate loss-of-lock rate predictions. For (b) the process is simple since these spectra are of a similar shape but of different magnitudes. For (c) the spectra are not of the same shape. The method proposed by the author involves finding the best fit single pole curve for the spectrum of the noise resolved with respect to the VCO and using the parameters of this curve in the calculations.

Practical measurement showed that errors in the analysis for the behaviour of the loops with large phase errors (of the order of π radians) and for multiple loss-of-lock events contributed approximately equally and oppositely to the loss-of-lock rate, for the system considered, and it was possible to ignore these effects in the comparison of predicted and measured loss-of-lock rates.

At present, both practical and analytical work indicate that the piecewise-linearization has an insignificant effect upon the accuracy of the calculations. It seems that inaccuracies occur because of the method of analysing the model and it is in this area that improvements can be made, both in accuracy and in ease of application of the analysis.

8. ACKNOWLEDGEMENTS

I am indebted to Dr. J. M. Badcock for the advice and encouragement he gave me throughout my studies at Monash University. I am also grateful for the support of the Australian Telecommunications Commission and for their permission to publish this paper.

9. REFERENCES

1. Badcock, J.M., "Thresholds in Communications Systems", Thesis for Ph.D. Monash University 1970. Chapter 4.

2. Rice, S.O., "Noise in F.M. Receivers", Bell System (L.1962). Proc. Symp. on Time Series Analysis. -ed. M. Rosenblatt. Wiley, N.Y. Chapter 25, pp.395-424, 1963.

3. Middleton, D., "An Introduction to Statistical Communications Theory". McGraw-Hill, N.Y. 1960.

4. Rice, S.O., "Mathematical Analysis of Random Noise", Bell System. Vol.23, July 1944 and Vol.24, January 1945. Reprinted in "Selected Papers on Noise and Stochastic Processes". N. Wax (Ed). Dover, N.Y. 1954, pp.133-294.

5. Smith, B.M., "Phase-locked Loop Threshold" Proc. IEEE (letters), Vol.54, pp.80-81, May 1966.

6. Ridgway, R.I., "Thresholds in Modulation Tracking Loops Employing Periodic Phase Detectors". T.R.W. Systems Report - No.2231-6009-Ru-000, July 1966, Page 8.

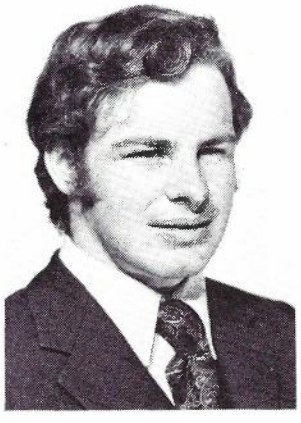

BIOGRAPHY

JAMES L. PARK was born in Geelong, Victoria, and graduated from Monash University with Honours in Electrical Engineering in 1971. He qualified for the degree of Master of Engineering Science in 1973 from the same University for work done on piecewise - linear modelling of phase-locked loops. Following the completion of his University studies he joined the Australian Telecommunications Commission Research Laboratories and is presently in the Devices and Techniques Section.

The Effect of the Ionosphere on the Phase of Standard Frequency Transmissions

K. H. JOYNER
L. C. BUTCHER
Division of Theoretical and Space Physics,
La Trobe University,
Bundoora, Victoria.

Standard frequency signals in the high frequency radio band are normally transmitted with very high accuracy. The received phase stability of such signals when propagated over any significant distance is, however, degraded by a number of effects peculiar to the dynamics of the ionosphere. This paper presents the results of phase measurements made on two standard frequency signals over short distances, discusses the parameters contributing to received phase instability and suggests techniques for identifying and removing such instabilities from phase measurements. The paper concludes with a discussion of a propagation time delay measurement technique which will be the basis of later work.

1. INTRODUCTION

Over the years, frequency and time information has been disseminated by CW radio transmissions (in the frequency range 2.5 - 25 MHz) which are locked to highly stable local oscillators. The shortcoming of this method of disseminating the information is that for signals to be propagated over any significant distance, propagation has to be via the ionosphere, and due to many dynamical processes occurring therein, the phase stability and accuracy associated with the signal becomes degraded. As the frequency standards have become better and better, so the effect of the ionosphere has become more important. In general the difference in frequency and phase between an oscillator and a signal derived from a second oscillator (which was originally synchronized with the first) which has been propagated via the ionosphere and compared with that oscillator is much less due to oscillator instability than it is to ionospheric effects. The ionospheric effects arise, in the simplest case, due to motion of the reflecting layer (giving a frequency (Doppler) shift) and due to refractive index changes along the path of the radio wave. The size of the ionospheric effect is known to vary with many parameters, e.g. time in the sunspot cycle, season, time of day and propagation distance.

At a given time of the day, not all the frequencies transmitted in the range 2.5 - 25 MHz get reflected from the ionosphere. For a receiver close to the transmitting source the higher frequencies penetrate the ionosphere near vertical incidence. But at a given location outside the skip zone (a zone outside which the ground wave is too weak to be received) better reception may be obtained on some frequencies than others. Hence several standard frequencies are usually transmitted from the same location in the hope that at least one signal may be received in any given location.

In this paper we discuss the results of measurements made on two transmissions (frequencies 2.5 and 4.5 MHz) both propagated via the ionosphere over short distances (approximately 50 km ground distance between transmitter and receiver). The measurements made were the changes in phase of the reflected wave compared to a local oscillator. We have monitored this change in the daytime for the 2.5 MHz signal, and the nighttime for the 4.5 MHz signal, for several months. From these measurements the effect of various dynamical ionospheric processes is estimated as a function of time of day, etc.. From such an analysis it is possible to either allow for or eliminate the ionospheric effects with some reliability at certain parts of the day and hence compare the two standards to a given accuracy with greater confidence than before.

The 4.5 MHz transmission is one of Telecom Australia's standard frequency transmissions, call sign VNG. The 2.5 MHz signal is derived from the VNG master oscillator and has the quality of a standard frequency transmission. It is of low power and is used only for experimental purposes. The carrier frequencies as transmitted remain within 1 part in 10^{10} of their nominal value.

2. EXPERIMENTAL TECHNIQUE

2.1 Propagation Modes

The 2.5 MHz signal was transmitted from Lyndhurst (38° 03'S, 145° 16'E) by Telecom Australia during the daytime (0900 - 1800 EST) and was received at La Trobe University (37° 43.5'S, 145° 03'E) for a period of 9 months-

a ground distance of approximately 50 km. During the daytime this signal is a one hop-transmission and is reflected from the E-region of the ionosphere (near 100 km altitude). The 4.5 MHz signal is also transmitted from Lyndhurst and was received also at La Trobe over a period of approximately 9 months. This signal is only transmitted at night (1945 - 0730 EST) and generally is an F-region reflection (probably from about 250 km). However there are times when this signal is reflected from sporadic E layers (E_s) and others when the signal is also returned from the ionosphere when the critical (i.e. penetration) frequency of the ionosphere is below 4.5 MHz (or more precisely when the parameter f x I - defined as the highest frequency for which F-region reflections are recorded, independent of whether they are from vertical or oblique incidence (Ref.1) falls below 4.5 MHz). Under this latter situation one would not expect the ionosphere to return any 4.5 MHz signal by a normal reflection and this situation will be discussed separately.

2.2 Receiver Arrangements

The parameter measured was the change in phase of the ionospherically reflected signal relative to a local stable oscillator at the receiving site. The offset and drift of the local oscillator at La Trobe could be measured daily since a 1 KHz signal derived from Telecom Australia's standard frequency installation was received at La Trobe by telephone line, and therefore could either be eliminated from the measurements or used to check the accuracy of the offset deduced. Both the 2.5 and 4.5 MHz signals were received using tuned loops as aerials. The advantage of such aerials is that with the plane of the loops vertical, little, if any, ground wave present would be induced in them, since the transmitting aerials were horizontal dipoles and the B vector of the ground wave would be vertical.

3. DAYTIME PROPAGATION

3.1 Phase Measuring System

Since the 2.5 MHz signal is reflected from the E-region the changes in phase measured are relatively slow and regular and so the method of measurement used was a mechanical phase locked servo-loop. This system has been described in detail elsewhere (Ref.2). Briefly, an output signal of 100 kHz is obtained from the receiver and phase detected against a 100 kHz signal derived from the local oscillator. The output of the phase detector is amplified and drives a small D.C. servo motor. After appropriate gearing this motor drives one side of a differential gearbox. The other side of this gearbox is driven by a synchronous motor which also derives its driving signal from the local standard. The offset of the D.C. amplifier is set such that in the quiescent state, i.e. zero output from the phase detector, the speeds of the two motors at the differential gearbox are equal and opposite so that the output of the differential gearbox is stationary. The output of the differential gearbox drives a magslip - whose outer coils are excited at 100 kHz derived from the local standard - and the magslip output is used as the standard for the phase detector. Thus as the phase of the receiver output changes, the D.C. motor rotates faster or slower - depending on whether the phase is changing positive or negative relative to the local standard - causing the centre element of the magslip to rotate in such a way as to reduce the phase difference between the local oscillator and receiver output signals. In fact if there is a constant small frequency difference Δf between the received and local oscillator signals, the magslip rotates at a constant rate Δf. By counting the number of revolutions of the D.C. motor in a given time, in this case 5 minutes, using a disc on the shaft with a small hole in it, with a small light and photo cell mounted on either side of the disc, the phase change occurring in that period may be measured. The number of revolutions of the motor was counted digitally and printed onto paper tape, all synchronizing signals being derived from the local oscillator. By suitable gearing one count different to the quiescent state count was equivalent to a phase change of $\pi/50$ in the 100 kHz output.

3.2 Phase Change Parameters

In general the results were as might be expected for an E-region reflection. Elementary theory indicates that the true height of reflection of a frequency f is determined by a term governing the production of the region by solar radiation of the form

$$h_f = h_{o_f} + H_f\{\log_e \sec X - \log_e (1 + \frac{2H_f}{N}\frac{dN}{dh})\} \qquad (1)$$

where h_o is a constant

H is the scale height

X is the solar zenith angle

N is the electron density which reflected the frequency f.

For the near vertically reflected 2.5 MHz signal the variation of $\frac{dN}{dh}$ with time (X) will be small near the central part of the day (Ref.3) and so the last term in the bracket of equation (1) may be considered constant and included in the h_o term. Thus we may re-write equation (1) as

$$h_f = h'_{o_f} + H_f \log_e \sec X. \qquad (2)$$

Besides this formation term, other perturbations exist which change the phase of the transmitted wave with time either by changing the reflection height or the refractive index along the path by redistributing electrons. These take the form of changes caused

(a) by the interaction with the earth's magnetic field of tidally induced currents associated with the solar, (S), and lunar (semi-diurnal), (L), magnetic variation

observed at the ground, and which flow in the E-region;

(b) by internal gravity waves propagating in the E-region. These typically have a dominant period in the E-region phase data of about 5 minutes (Ref.4);

(c) small scale irregularities in the ionization and short lived E_s patches.

Hence we may incorporate these effects into Equation (2) to give us the change in phase ΔP in unit time (5 minutes in this case) of the form

$$\Delta P = 2H_f \tan X \Delta X \pm (\Delta P)_S \pm (\Delta P)_L \pm (\Delta P)_{IRREGS} \pm (\Delta P)_{\substack{GRAVITY \\ WAVES}} \pm (\Delta P)_{OFFSET} \quad (3)$$

where we have assumed that h'_{o_f} is constant, and the symbol Δ indicates the changes taking place in a 5 minute period. $(\Delta P)_{OFFSET}$ is the phase difference occuring in the 5 minute period due to the slight difference in the transmitting and receiving reference oscillators. (The factor 2 appears since the wave traverses the medium twice - once on the way up and once down). It should also be noted that the term $(\Delta P)_{GRAVITY\ WAVES}$ is not always present. $(\Delta P)_S$ is present to a greater or lesser extent most of the time, although it is possible to select days when it is negligible. The term $2H_f \tan X\ \Delta X$ is by far the largest for most of the day. Only in the two hour period centred on $X = X_{MIN}$ (or $\Delta X = 0$) is it possible usually for the other terms to dominate. Of these, at our latitudes $(\Delta P)_S$ is the largest, when present, although $(\Delta P)_{IRREGS}$ is unpredictable and can become surprisingly large at any time. This is particularly true if sporadic E is present moving in the horizontal or vertical direction.

3.3 Discussion

By observing the phase change ΔP, the contributions of the terms in equation (3) may be estimated and then eliminated which allows the difference between the two oscillators to be determined. Alternatively, a method of analysis may be used which eliminates some of the terms, while the contributions of others may be estimated. This latter method would appear to be most obvious, since the contributions of some terms may vary with time, place and conditions and it would therefore be advantageous to eliminate them; whilst others are known to a good approximation and probably do not vary appreciably. The two easiest terms to eliminate are the terms $(\Delta P)_{GRAVITY\ WAVES}$ and $(2H_f \tan X\ \Delta X)$. It is well known (see, for example, (Ref.4)) that $(\Delta P)_{GRAVITY\ WAVES}$ is both small and regular in period, when present. Since the period of these waves is approximately 5 minutes, the collection of data over five minute periods eliminates this term.

The term $2H_f \tan X\ \Delta X$ is the largest term contributing to ΔP in equation (3). It may be determined by plotting $\tan X\ \Delta X$ versus ΔP which should render a straight line the gradient of which gives a value of H_f. However, for a single day's data, a certain amount of scatter in the points - due to the other terms in equation (3) - make it difficult to get an accurate value of H_f. If a value of H_f is obtained in this way, the value of $(\Delta P)_{OFFSET}$ obtained at a given time as $(\Delta P - 2H_f\ \Delta X \tan X)$ will in general be in error by $\mp |(\Delta P)_S \mp (\Delta P)_L \mp (\Delta P)_{IRREGS}|$ since these terms are not determined or eliminated. However, since $(\Delta P)_S$ only makes its presence felt near the central part of the day (Ref.5), its contribution may be eliminated by doing the calculation at a time away from one central part of the day. The terms $(\Delta P)_L$ and $(\Delta P)_{IRREGS}$ are difficult to eliminate, since $(\Delta P)_{IRREGS}$ is a random component and, although the maximum value of $(\Delta P)_L$ expected is approximately $\pi/2$ radians/5 minute intervals (Ref.6), its actual contribution will depend on lunar time. (It may be eliminated since $(\Delta P)_L$ is periodic with a period of 12 lunar hours and has a maximum of $\pi/2$ radians/5 minute intervals occurring at about 1000 hours (lunar time)). If the average value of ΔP at given times is taken over a 14-15 day period, the terms $(\Delta P)_{IRREGS}$ and $(\Delta P)_L$ are eliminated; $(\Delta P)_{IRREGS}$ because the irregularities causing contributions to ΔP occur more or less randomly and $(\Delta P)_L$ because lunar time regresses at a rate of 50 minutes per (solar) day.

A plot of $(\Delta P)_{AV}$ against the average $\tan X\ \Delta X$ for a 2 week period is shown in Fig.1. We see that outside the central part of the day, the points may be fitted by two straight lines, one for the morning data and one for the afternoon data, each with different gradients, i.e. different H_f s. (This effect has been reported and discussed before in Refs. 3 and 5).

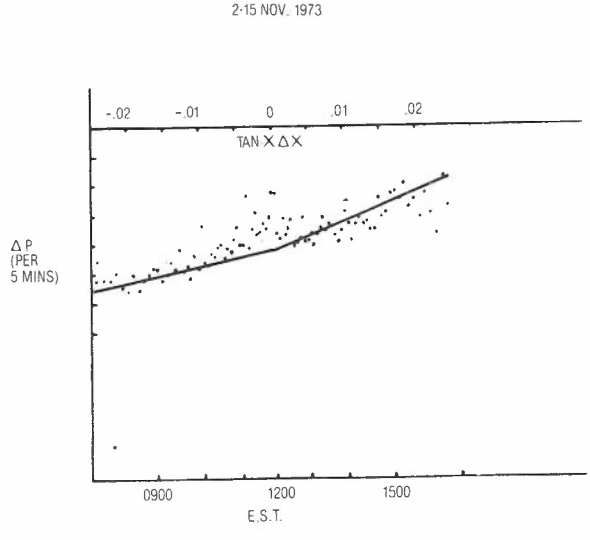

Fig.1 - Average Phase Change in a 5 Minute Period (averaged over 2 weeks) Determined at $\Delta X = 0$ for 2.5 MHz.

The obvious deviations from the straight lines are due to the effect of $(\Delta P)_S$, which usually only makes its presence felt during the central part of the day. However its effect may be eliminated by measuring ΔP where the straight line fit meets the tanχ Δχ = 0 line which gives $(\Delta P)_{OFFSET}$ directly. Some inaccuracy arises due to the fact that χ changes slowly over the two week period, but this will not affect the result significantly. Also, $(\Delta P)_{OFFSET}$ calculated in this way is the average over a two week period. If one assumes that the local oscillator is drifting at a linear rate, then this average value corresponds to the offset applicable to the central day of the period. Hence repeating such an exercise using days 1-15, 2-16, 3-17, ..., etc. indicates the offset on days 8, 9, 10, ... etc.. A plot of this offset against day number would then allow one to predict the offset of later days, assuming a constant drift rate of the offset. This may be seen in Fig.2 where the average of ΔP is plotted against the offsets measured and the predicted offsets indicated by the line of best fit through those parts may be compared with the actual values measured daily.

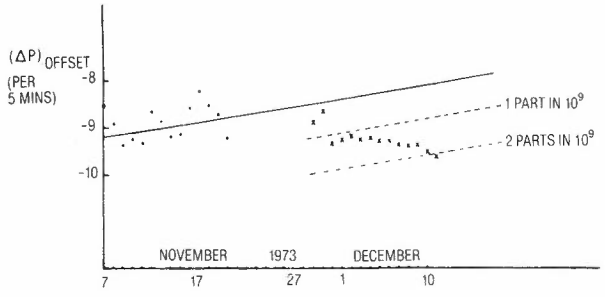

Fig.2 - Predicted Future Average Offset (straight line) Determined from One Months Measured Values (.) and the Actual Offset Measured Later (x) for 2.5 MHz.

It may be seen that the offset predicted by the line of best fit in Fig.2 is not drifting in the same direction as the actual measured values taken later. (This would appear to be due to a "jump" in our standard around November 30 - December 1). However, we see that even so the predicted values at a two week lag are still only in error by 2 parts in 10^9. Continual updating of the data would take account of the change in direction of the drift. This method is really only useful in the summer where the E-region tends to behave fairly regularly.

This method of determining ΔP at tanχ Δχ = 0 may also be used for single days, as long as the scatter in the points is low enough for a line of best fit to be meaningful. An example is shown in Fig.3 and a plot of the error as a function of the day (when an offset could be determined in this way) is shown in Fig.4. Most determinations made in this way are also confined to the summer and give errors of up to approximately 5 parts in 10^9.

A third, less tedious method involves eliminating the term $2H_f$ tanχ Δχ from equation (3). This may be done since the term is symmetrical about Δχ = 0 (or at least approximately so if we take a small enough period when H_f may be

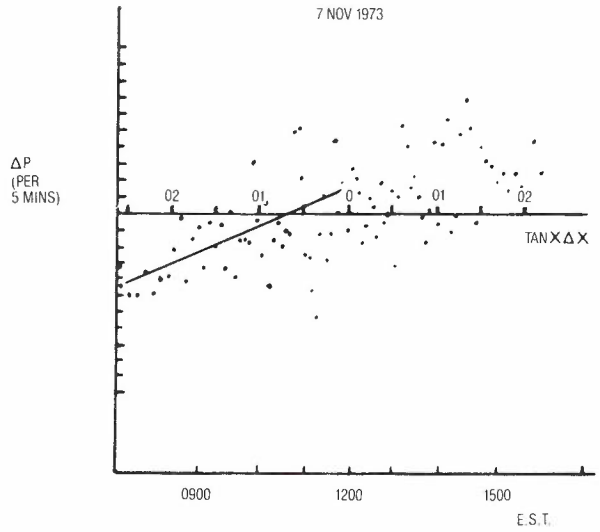

Fig.3 - Phase Change in a 5 Minute Period (for a single day) Determined at Δχ = 0 for 2.5 MHz.

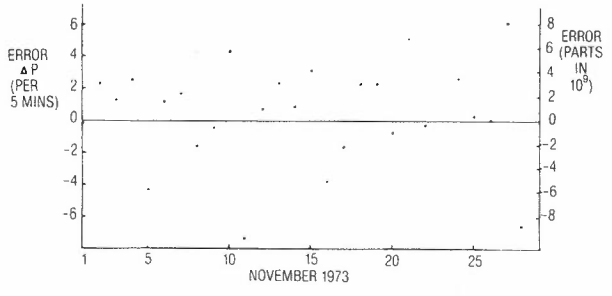

Fig.4 - Measured Phase Error between the Received and Transmitted Signals Determined from the Daily Measurements at Δχ = 0 during November 1973 for 2.5 MHz.

assumed constant). Thus adding all the (ΔP)'s over a period of say one hour - half hour each side of the Δχ = 0 time - eliminates $2H_f$ tanχ Δχ. This method is by far the simplest and gives fairly good results. This is seen from Fig.5 which plots the phase error (and stability) for the whole period of observation.

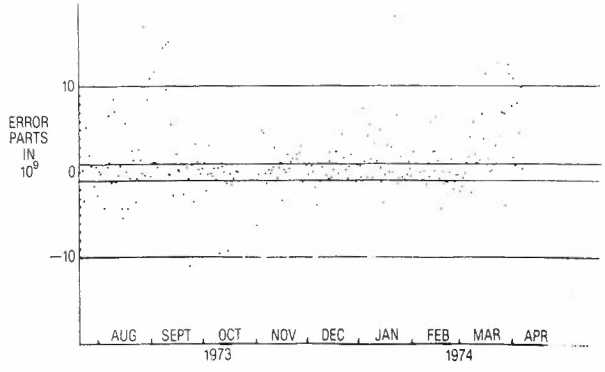

Fig.5 - Measured Phase Error between the Received and Transmitted Signals Determined by Averaging the Phase Change over the Period 30 Minutes either Side of Δχ = 0 for 2.5 MHz.

In this data the term $(\Delta P)_L$ was not allowed for (since it is a small term anyway) and hence the error represents $\mp (\Delta P)_S \mp (\Delta P)_{IRREGS} \mp (\Delta P)_L$. From this data, we see that on 44% of occasions the offset error is less than 1 part in 10^9, and on 6% of occasions is greater than 1 part in 10^8. This error might be expected to be less over larger oblique paths. This improvement occurs due to two reasons.

(a) The signal is reflected lower down in a more stable part of the E-region ($\frac{dN}{dh}$ is approximately constant with time).

(b) The propagation angle i is greater and the change in the phase δP_{if} of a signal propagated obliquely in the E-region at frequency f is related to the change in the phase δP_{ofcosi} on a signal transmitted vertically on the equivalent vertical frequency fcosi by the approximate relation (Ref.2)

$$\delta P_{if} = \text{cosi } \delta P_{ofcosi}. \qquad (4)$$

This implies that for any effect in the ionosphere that effects the phase, such as a height change of the layer, the change of phase will be smaller at larger values of the angle i. The further the receiver is from the transmitter, the larger i will be. However, if the receiver is too far away, the propagation may be via a two hop mode. Although the above principles involved in measuring $(\Delta P)_{OFFSET}$ should hold in this case also, the accuracy would probably be less, since the wave would have to transverse the ionosphere twice, and hence any effect on the phase would be doubled. Also i would be decreased. The other problem is that one may get a mixture of one and two hop propagation and this would make the analysis outlined above difficult. Whether a one or two hop propagation dominates will depend on the relative absorption along the two propagation paths, and this will change as the electron density profile changes (i.e. with time of day). However, it is fairly safe to say that a one hop mode will dominate up to a distance of approximately 600-800 kms.

4. NIGHTTIME PROPAGATION

4.1 Phase Measuring System

With the 4.5 MHz transmission at night, propagation was via the F-region. The F-region at night is a lot more unstable than the E-region in the day, and the phase changes involved are too fast and variable to be measured in the manner used for the 2.5 MHz. Instead, the local 100 kHz was offset by 5 Hz and this was phase detected against the 100 kHz from the receiver, the result again being punched on paper tape every minute. This enabled positive and negative phase changes to be measured up to ± 5 Hz, which was well within the range observed by other methods.

4.2 Phase Change Parameters

It should be noted at these frequencies, and particularly at night, two magnetoionic components are propagated, the o-ray and the e-ray. Since each is propagated independently, the phase changes associated with each mode are different. Hence the two modes must be separated otherwise they will beat and spurious phase (and amplitude) changes will arise. The two modes are not a problem at 2.5 MHz since the relative amplitudes of the two components is mainly determined by the non-deviative absorption, A, for the two modes which is given by

$$A \propto \frac{1}{(f \pm f_H)^2} \qquad (5)$$

where f is the frequency of propagation

f_H is the gyrofrequency and is approximately equal to 1.5 MHz, and the + and - sign refer to the o-ray and e-ray respectively. Hence we see that $(A_e/A_o)_{2.5} \sim 16{:}1$ whereas $(A_e/A_o)_{4.5} \sim 4{:}1$. Since the two modes are oppositely circularly polarized, either may be eliminated in the receiver system. The results presented here were obtained separately on both o- and e-rays.

The equation that governs the change in phase in this case is of the form

$$\Delta P = (\Delta P)_{\substack{\text{BULK} \\ \text{CHANGES}}} \pm (\Delta P)_{\substack{\text{GRAVITY} \\ \text{WAVES}}} \pm (\Delta P)_{IRREGS} \pm (\Delta P)_{OFFSET}. \qquad (6)$$

In this case $(\Delta P)_{BULK\ CHANGES}$ includes changes caused by ionization variations along the ray path and vertical motions. It is a difficult term to eliminate as it is not regular.

4.3 Discussion

The first two terms in equation (6) may be very large and dominate. Their relative magnitudes may change during the night, but in general $(\Delta P)_{BULK\ CHANGES}$ dominates most of the time. Also, both may be very variable, the gravity wave period being found to be anywhere in the range from a cut-off period around 15 minutes (the Brunt Vaisälla period), to about 60 minutes. Also, the gravity wave contribution was found to be present to a greater or lesser extent on almost every night at least for part of the night. The size of $(\Delta P)_{GRAVITY\ WAVES}$ was found to be related to the magnetic Kp index - since most are thought to have originated in the southern auroral regions - and so the best nights to measure $(\Delta P)_{OFFSET}$ are those when Kp is low. An example indicating the presence of the gravity wave component is shown in Fig.6. The procedure again was to average the ΔP's over the period of an oscillation thus eliminating the gravity wave effect. In general this average was not zero, and the value gave $(\Delta P)_{OFFSET} \mp (\Delta P)_{BULK\ CHANGES} \mp (\Delta P)_{IRREGS}$. This error to $(\Delta P)_{OFFSET}$ could be quite large and is

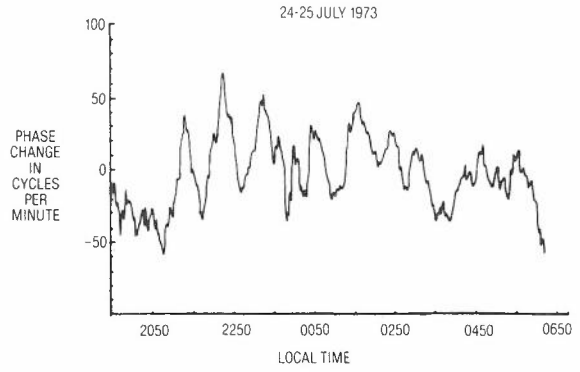

Fig.6 - Phase Change in a 1 Minute Period for the 4.5 MHz Transmission as a Function of Time Indicating the Presence of Gravity Waves.

difficult to eliminate. Using this method the errors in the measured offset were large.

Using only data where a dominant gravity wave period was indicated through spectral analysis, the data was averaged over two of those periods centred on midnight. This was carried out for the four summer months of 1973-1974 (November - February) and it was found that all the days gave errors of less than 5 parts in 10^8 and 50% gave errors of less than 2 parts in 10^8. These results are not as good as the 2.5 MHz results, which is not surprising since the F-region is not as stable or regular as the E-region. There appears no simple way of reducing this large error at this stage.

As mentioned earlier, sometimes the index F x I fell below the frequency of transmission. In this case, signals were still received, although their phases were quite unstable and jumped around. It was found that this mode of propagation was a scatter mode from irregularities near the F-2 peak. This scatter mode is easily identified if amplitude variations are monitored and the effect has been discussed in detail (Ref.7). Of course, as the receiver distance is increased, the signal is propagated at a more oblique angle and f x I will tend more to stay above the equivalent vertical frequency.

5. TIME DELAY MEASUREMENTS

The 4.5 MHz (and the 7.5 MHz and 12.5 MHz) transmission from Lyndhurst has a 1 kHz modulation on it every second, 50 msec long, although longer on the minute. This pulse may be used for time synchronization between receiving stations, although the pulse takes a variable time to reach receiving stations since it is propagated via the ionosphere. The time delay t is given by

$$t = \frac{P'}{c} \qquad (7)$$

where P' is the group path of the pulse and is given by

$$P' = 2 \int_{\text{path}} \mu' dh \qquad (8)$$

and μ' is the group refractive index and depends in a very complex way on the electron density along the path (Ref.8). Because one does not know the exact time of transmission of the pulse, it is very difficult to measure the time delay correctly. The variation in time between consecutive pulses may be measured, but due to ionospheric effects such as fading, which causes the rise time of the pulse to vary, it is difficult to measure the variability in time between the pulses to any accuracy.

It should be possible to improve the accuracy of measurement of P' over the path (i.e. t) or the error in the true interval Δt between the one second pulses received using a method based on that suggested by Whitehead and Malek (Ref.9). This method involves measuring the change in phase $\Delta\phi$ with frequency of two waves propagated over the same path. It may easily be shown (Ref.9) that the group delay P' is given by

$$P' = \frac{c}{2\pi} \frac{\Delta\phi}{\Delta f} . \qquad (9)$$

when Δf is the frequency interval over which $\Delta\phi$ is measured

$$\therefore \quad t = \frac{1}{2\pi} \frac{\Delta\phi}{\Delta f} \qquad (10)$$

and $P' = ct$.

Since we may write $\Delta\phi = 2\pi n + \alpha$ then

$$t = \frac{1}{2\pi} \left(\frac{2\pi n + \alpha}{\Delta f}\right) \qquad (11)$$

where n is an integer. We see that for f = 1kHz (as is the case with double side band transmissions from Lyndhurst) then

$$t = 1000\left(n + \frac{\alpha}{2\pi}\right) \text{ μsecs.} \qquad (12)$$

We see that if we know t to within $\mp$ 500 μsecs, then we may determine n and hence t. We see that a change in phase of 2π radians is equivalent to a change in t of 1000 μsecs. Therefore measurement of $\Delta\phi$ to an accuracy of $2\pi/100$ rads allows t to be measured to $\mp$ 10 μsecs.

Even if t is not known to within $\mp$ 500 μsecs at least the error in the time between two consecutive one-second pulses may be determined. Since a phase change of 2π between consecutive one-second pulses is equivalent to a time difference of 1 msec, (which is very much larger over all practical paths) then the integer n would be the same for two measurements made one-second apart. Then

$$\Delta t = \frac{10^3}{2\pi} (\alpha_{t_1} - \alpha_{t_2}) \text{ μsecs} \qquad (13)$$

(We can see from equation (12) that in principle the larger Δf the more accurate we can measure t and Δt. However, we cannot increase Δf indefinitely since equation (9) is only valid if the waves travel (approximately) the same path and also the larger Δf becomes the more difficult it is to determine n in equation (12) and it becomes more likely that n will not be constant between successive pulses in determining Δt. However, a Δf of up to about 10 kHz should be acceptable).

An experiment based on the above principles to measure τ is at present being built at La Trobe University and it is hoped to present results in the not too distant future.

ACKNOWLEDGEMENT

This work was supported by a grant from the Australian Radio Research Board. One of us (KHJ) would like to acknowledge the receipt of a Commonwealth Postgraduate Award during the period of this work.

REFERENCES

1. Piggott W.B. and Rawer K., "URSI Handbook of Ionogram Information and Reduction", 1972, 2nd edition.

2. Butcher E.C. and Weekes K., "Journal of Atmospheric and Terrestrial Physics", 1969, Vol.31, p.1421.

3. Rodgers R.P. and Butcher E.C., to be published in "Journal of Atmospheric and Terrestrial Physics".

4. Vincent R.A., "Journal of Atmospheric and Terrestrial Physics", 1969, Vol.30, p.607.

5. Butcher E.C., "Journal of Atmospheric and Terrestrial Physics", 1970, Vol.32, p.97.

6. Joyner K.H., "Ph.D. Thesis", 1976, La Trobe University, Bundoora, Victoria, Australia.

7. Cornelius D.W., Joyner K.H., Dyson P.L. and Butcher E.C., "Journal of Atmospheric and Terrestrial Physics", 1975, Vol.37, p.609.

8. Davies K., "Ionospheric Radio Waves", Blaisdell Publishing Co., 1969, p.132.

9. Whitehead J.D. and Malek A., "Journal of Atmospheric and Terrestrial Physics", 1963, Vol.25, p.599.

BIOGRAPHIES

E. C. BUTCHER - B.Sc. (hons) - University of Exeter, U.K. 1962. Ph.D in Ionospheric Physics - University of Exeter, 1966. Employed as research scientist 1965-1968 at G.E.C. Hirst Research Centre, Wembley, U.K. - worked on optical properties of surfaces. Joined La Trobe University, 1968. Present position: Senior Lecturer in Division of Theoretical and Space Physics.

K. H. JOYNER - B.Sc. (hons) - La Trobe University, Australia, 1971. Ph.D in Ionospheric Physics, La Trobe University, 1976. Present position: Head of Senior Sciences, Templestowe Technical School.

The Calculation of the Power Spectral Density of 24-Channel PCM Systems When in the Idle Condition

B. M. SMITH
Telecom Australia Research Laboratories

In this paper an idealized model of the idling condition of a 24-channel PCM system is presented and from this model the power spectral density of the line signal is derived. Knowledge of this power spectral density is required in systems studies of the penetration of PCM systems into junction cable routes and also in the calculation of the crosstalk interference of the PCM line signals into other services in the junction cable. The results indicate that when idling the power spectrum of the PCM signal is significantly more concentrated near its maximum value (which occurs close to half the line rate) than when carrying random digital signals.

1. INTRODUCTION

The use of primary level PCM systems on junction cable routes is one method of increasing the capacity of these routes. To efficiently plan the installation of such systems, information is required on how they interact with each other and with other services in the junction cable. One important parameter that determines this interaction is the power spectral density of the PCM signal and in this paper we consider the power spectral density when the PCM system is in the idling condition. Only 24-channel PCM systems are considered in this paper (Refs. 1 and 2).

2. THE PCM LINE SIGNAL

24-channel PCM systems use alternate-mark-inversion (AMI) coding for the line transmission. In this code 'ones' are transmitted as pulses of alternating polarity while 'zeros' correspond to an absence of pulses. Although this description has great simplicity, we find an alternative description to be much more fruitful when deriving the properties of the transmitted signal. This alternative description treats the AMI signal as a form of partial response (PR) coding (Refs.3, 4 and 5) where the digital stream is precoded before the PR coder and pulse shaper. For AMI coding, the method is shown in Fig.1 where $\{a_n\}$ is the input digital sequence, $\{b_n\}$ is the precoded digital sequence, 1-D is the AMI PR coder

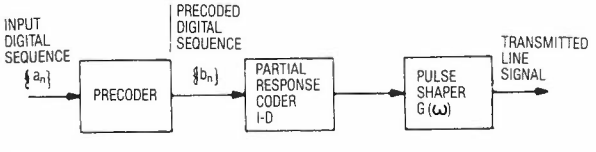

Fig. 1 - AMI Line Coding as a Form of Partial Response Signalling.

(D is the delay operator) and $G(\omega)$ is the pulse shaper. The precoder operation is given by

$$b_n = b_{n-1} \oplus a_n \qquad (1)$$

where $\oplus$ = modulo 2 addition

and a_n, b_n = 0, 1.

$G(\omega)$ is chosen to give half-width pulses (i.e. T/2 where T^{-1} = 1.544 MHz); these pulses are also half-height which are then converted to full height by the 1-D coding.

The important advantage of this method of representation of the AMI signal is that only linear operations are performed on the digital sequence, $\{b_n\}$, to give the transmitted signal. However, it then becomes necessary to determine the properties of the precoded sequence $\{b_n\}$ for a given input sequence $\{a_n\}$.

3. SOME RESULTS FOR THE PRECODED DIGITAL SEQUENCE

In this section, we derive some useful properties of the precoded sequence $\{b_n\}$, given that the original sequence $\{a_n\}$ is statistically independent and has the following probabilities:

$$\text{prob}\,(a_n = 1) = p$$

$$\text{prob}\,(a_n = 0) = 1-p$$

At this stage it is convenient to transform the elements of the digital sequences $\{a_n\}$ and $\{b_n\}$ as follows:

$$1 \rightarrow -1$$

$$0 \rightarrow +1$$

and thence:

$$\text{prob } (a_n = 1) = 1-p$$

$$\text{prob } (a_n = -1) = p$$

that is p is the probability of that input symbol which changes the output state of the precoder.

The modulo-2 operation then becomes:

$$b_n = b_{n-1} \, a_n \qquad (2)$$

that is the modulo-2 addition has been replaced by multiplication which is much easier to handle in the derivation of correlation functions. Firstly, consider the probability of an element of $\{b_n\}$. Let

$$\text{prob } (b_n = 1) = q$$

$$\text{prob } (b_n = -1) = 1-q$$

and because of the independence of $\{a_n\}$ we can write the joint probability:

$$\text{prob } (b_{n-1}, a_n) = \text{prob } (b_{n-1}) \text{ prob } (a_n) \qquad (3)$$

and hence

$$\text{prob } (b_n = +1) = \text{prob } (b_{n-1} = 1) \text{ prob } (a_n = 1) + \text{prob } (b_{n-1} = -1) \text{ prob } (a_n = -1) \qquad (4)$$

$$q = q(1-p) + (1-q)p \qquad (5)$$

which can be solved to give q = 0.5. That is the elements of the precoded sequence are equiprobable even if $\{a_n\}$ is not. However, the sequence $\{b_n\}$ is correlated as follows:

The auto-correlation of $\{b_n\}$ is:

$$R_b(m) = E \, (b_{n+m} \, b_n) \qquad (6)$$

and invoking (2)

$$R_b(m) = E \, (b_{n+m-1} \, a_{n+m} \, b_n). \qquad (7)$$

Successive further substitution of (2) leads to

$$R_b(m) = E \, (a_{n+m} \ldots\ldots a_{n+1} \, b_n \, b_n) \qquad (8)$$

and using the independence of $\{a_n\}$

$$R_b(m) = [E(a)]^m \qquad (9)$$

$$= [1.(1-p) + (-1)\, p]^m$$

$$= [1-2p]^m \qquad (10)$$

where p is the probability of a pulse. It may be noted that for p = 0.5,

$R_b(m) = 0 \quad (m \neq 0)$ and $\{b_n\}$ becomes an equiprobable uncorrelated sequence as we would expect from entropy considerations.

Reverting back to the more general case with p not necessarily equal to 0.5, the importance of the above result is that unequal probabilities in the sequence $\{a_n\}$ give a linear effect in $\{b_n\}$; this can be cascaded with the 1-D and G(ω) operations in the AMI generation (see Fig.1).

Taking the Fourier transform of $R_b(m)$ gives

$$C(\omega) = 1 + e^{j\omega T}(1-2p) + e^{j\omega 2T}(1-2p)^2 + \ldots + e^{-j\omega T}(1-2p) + e^{-j\omega 2T}(1-2p)^2 + \ldots$$

$$= \frac{4p(1-p)}{1 + 2\cos\omega T\,(2p-1) + (2p-1)^2} \qquad (11)$$

which is cascaded with 1-D and G(ω). The above results are also given in (Ref.5).

For completeness we now derive the cross-correlation of the sequences $\{a_n\}$ and $\{b_n\}$. This result is used in calculating the AMI spectrum with unequal positive and negative pulse shapes and, also, the spectrum of the two-level AMI class 1 code (Ref.4).

Consider the cross-correlation

$$R_{ab}(m) = E \, (b_n \, a_{n+m}) \qquad (12)$$

and the following two cases:

(1) $m \geq 1$

Since a_{n+m} is independent of b_n

$$E \, (b_n \, a_{n+m}) = E \, (b_n) \, E \, (a_{n+m})$$

$$= 0 \qquad (13)$$

$(E \, (b_n) = 0$ as b_n is equiprobable)

(2) $m < 1$

$$E \, (b_n \, a_{n+m})$$

$$= E \, (b_{n+m-1} \, a_{n+m} \ldots a_{n-1} \, a_n \, a_{n+m})$$

$$= E \, (b_{n+m-1}) \, E \, (a_{n+m}^2) \ldots E \, (a_{n-1}) \, E \, (a_n)$$

$$= 0 \qquad (14)$$

since $E \, (b_{n+m-1}) = 0$

Hence, the cross-correlation of $\{a_n\}$ and $\{b_n\}$ is zero.

4. PCM SIGNAL WITH IDLING

The 24-channel PCM signal (Ref.2) consists of 24 8-bit words in a frame together with a 193rd bit for frame alignment and for multiframe alignment or signalling. The multiframe consists of 12 frames. If the 193rd bit is not used for signalling, then it has the pattern shown in Table 1.

TABLE 1 - Pattern of 193rd Bit in the Multiframe

Frame Number	193rd Bit
1	1
2	0
3	0
4	0
5	1
6	1
7	0
8	1
9	1
10	1
11	0
12	0

In addition, in the 6th and 12th frames, every 8th bit (LSB) in each of the 24 8-bit words is reserved for signalling purposes; in the idle condition these bits are set to 'one'. A summary of the above information is shown in Fig.2.

The 24-channel PCM system uses the μ-law encoding for the analogue-to-digital conversion (Ref.1). With this law, the output words from the encoder for the quantization steps close to zero are shown in Table 2.

TABLE 2 - Output Words for Quantization Steps Near Zero

Level	Word							
	1 Sign Bit	2 MSB	3	4	5	6	7	8 LSB
+7	1	1	1	1	1	0	0	0
+6	1	1	1	1	1	0	0	1
+5	1	1	1	1	1	0	1	0
+4	1	1	1	1	1	0	1	1
+3	1	1	1	1	1	1	0	0
+2	1	1	1	1	1	1	0	1
+1	1	1	1	1	1	1	1	0
0+	1	1	1	1	1	1	1	1
0-	0	1	1	1	1	1	1	1
-1	0	1	1	1	1	1	1	0
-2	0	1	1	1	1	1	0	1
-3	0	1	1	1	1	1	0	0
-4	0	1	1	1	1	0	1	1
-5	0	1	1	1	1	0	1	0
-6	0	1	1	1	1	0	0	1
-7	0	1	1	1	1	0	0	0

In the idle condition, the PCM codec samples a nominal zero signal; however, due to noise and offset voltages, the actual value being sampled may not be zero. Some experimental results for the idle words of each channel of a 24-channel PCM are given in the Appendix. It is evident that the effect of the noise and offset differs for each channel. For example, one channel has remained in the same state while other channels move through up to four states with, in general, unequal probabilities of being in each state. A simple and complete characterization of the idle-word behaviour as shown in the example given in the Appendix does not seem feasible. We have decided to restrict our attention to an idle word behaviour model where each channel can independently select one of a pair of idle words with the same pair for each channel. However, we do permit an unequal probability of selection of the idle words. In this paper we propose to evaluate the average power spectrum of line signal when idling with unequal probability between the two zero levels (0+ and 0- in Table 2) including the effect of the stolen bits in the 6th and 12th frames and the 193rd bit (with equal probabilities only). The paper also evaluates the spectra for other combinations of pairs but not including the effects of the stolen and 193rd bits, or unequal probabilities.

5. CALCULATION OF AVERAGE POWER SPECTRUM WHEN IDLING

5.1 Random Selection of the Two Zero Levels

In this case the input to the precoder is an independent randomly selected choice of the words:

11 11 11 11

and 01 11 11 11

corresponding to the two zero levels in the μ-law encoder. The LSB in each of these words is a '1' which is identical to the replacement bit in the 6th and 12th frames and, hence, we can ignore the stolen bit in these frames in this particular case.

For the time being let us ignore the 193rd bit and assume the probabilities of the above words

$$\text{prob}(11\ 11\ 11\ 11) = 1-p \qquad (15)$$

$$\text{prob}(01\ 11\ 11\ 11) = p \qquad (16)$$

It is easy to show that after the precoder the words become

10 10 10 10

and 01 01 01 01

and from the results in Section 2 these words are equiprobable but correlated. The form of the correlation is given by equation (10). It should be noted that we have adopted the convention for probabilities in (15) and (16) as stated in Section 8, viz. p is the probability of that word (or symbol) which changes the state of the word (or symbol) at the output of the precoder. That is when the PCM system is idling between the two zero states, the precoded sequence $\{b_n\}$ in Fig.1 becomes a sequence of equiprobable but correlated 8-bit words which then become the input to the PR coder, 1-D, and the pulse shaper.

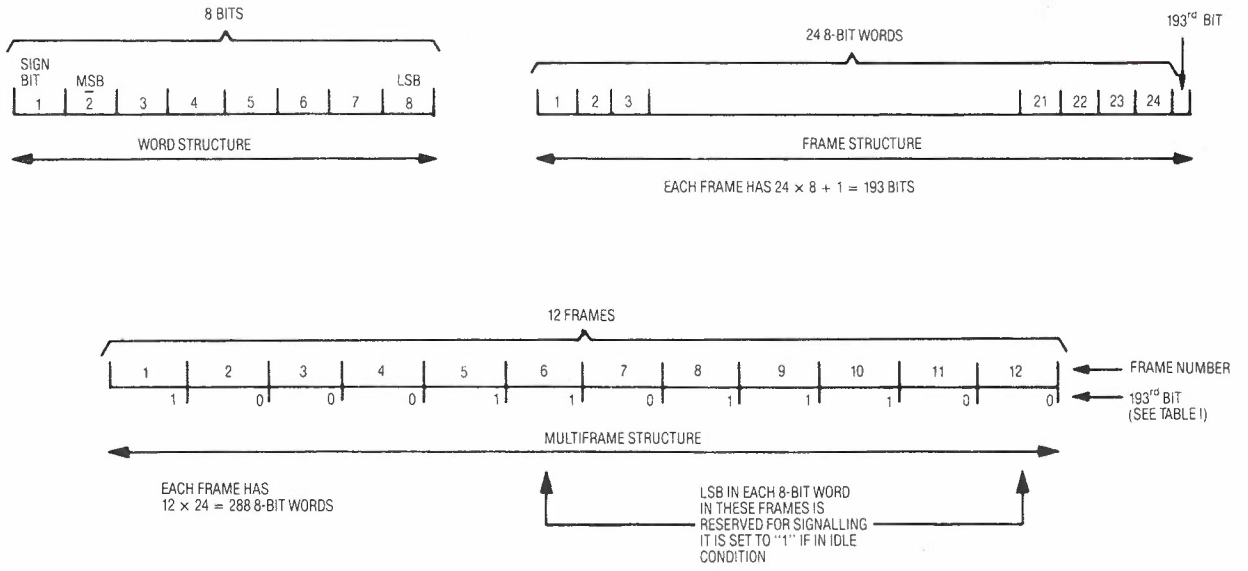

Fig. 2 - 24-Channel PCM Frame and Multiframe Structure.

Furthermore, if we adopt the transformation, as before, of

$1 \rightarrow -1$

$0 \rightarrow +1$

then the 8-bit words become

$-1 \quad +1 \quad -1 \quad +1 \quad -1 \quad +1 \quad -1 \quad +1$

and $+1 \quad -1 \quad +1 \quad -1 \quad +1 \quad -1 \quad +1 \quad -1$

and, hence, we have a basic word $-1\ +1\ -1\ +1\ -1\ +1\ -1\ +1$ being multiplied by ± 1. The system can then be modelled as in Fig.3

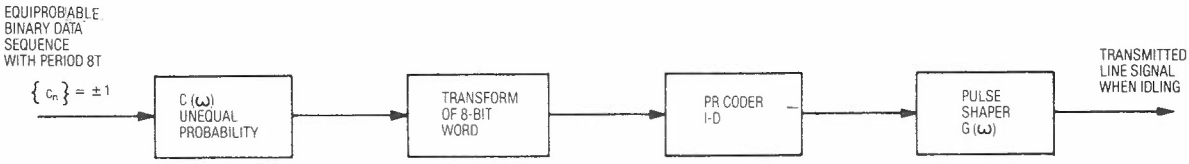

Fig. 3 - Idealized Model of 24-Channel PCM System Line Signal when Idling.

where an uncorrelated equiprobable binary data signal is followed by four linear operations corresponding to the:

(i) correlation due to $p \neq 0.5$, $C(\omega)$

(ii) Fourier transform of 8-bit word

(iii) 1-D coder

(iv) pulse shaper, $G(\omega)$

The Fourier Transform of the PR (1-D) coder is given by $e^{j\omega T/2} - e^{-j\omega T/2}$, and the Fourier transform of the pulse shaper $G(\omega)$ for a half-width pulse (and half height), $g(t)$, as shown in Fig.4 is given by

$$G(\omega) = \int_{-\infty}^{\infty} g(t)\ e^{-j\omega T} dt \qquad (17)$$

$$= \frac{AT}{4} \left[\frac{\sin\omega T/4}{\omega T/4}\right] \qquad (18)$$

This pulse is made to be half the height of the output PCM pulse as the 1-D coder doubles the peak pulse height.

The Fourier transform of the basic word, $-1\ +1\ -1\ +1\ -1\ +1\ -1\ +1$ is given by

$$W(\omega) = e^{j\omega T/2} - e^{-j\omega T/2} - e^{j\omega 3T/2} + e^{-j\omega 3T/2}$$

$$+ e^{j\omega 5T/2} - e^{-j\omega 5T/2} - e^{j\omega 7T/2} + e^{-j\omega 7T/2}$$

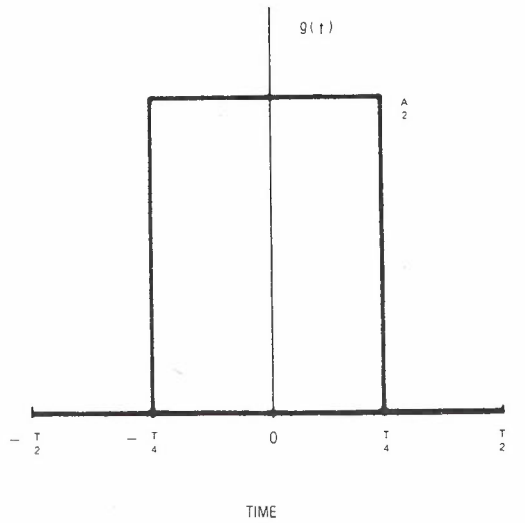

Fig. 4 - Half-width Pulse Shape for PCM Line Signal.

$$=2j(\sin\omega T/2 - \sin 3\omega T/2 + \sin 5\omega T/2 - \sin 7\omega T/2) \quad (19)$$

and, hence, the power spectrum of the output signal becomes

$$P(\omega) = \frac{1}{8T}\frac{1}{R}\frac{A^2T^2}{16}\left[\frac{\sin\omega T/4}{\omega T/4}\right]^2 4\sin^2\omega T/2 \cdot \frac{4p(1-p)}{1+2\cos 8\omega T(2p-1)+(2p-1)^2} \cdot 4(\sin\omega T/2 - \sin 3\omega T/2 + \sin 5\omega T/2 - \sin 7\omega T/2)^2$$

$$= \frac{A^2T}{2R}\left[\frac{\sin\omega T/4}{\omega T/4}\right]^2 \sin^2\omega T/2 \cdot \frac{p(1-p)}{1+2\cos 8\omega T(2p-1)+(2p-1)^2} \cdot (\sin\omega T/2 - \sin 3\omega T/2 + \sin 5\omega T/2 - \sin 7\omega T/2)^2 \quad (20)$$

The normalized, $P(\omega)$, is plotted in Fig.5 for various values of p and indicates how the shape of each lobe in the spectrum is highly dependent on p (Note: p is the probability of the 0- state).

The idling condition model in Fig.3 can be extended to include the 193rd bit. The effect of the 193rd bit is to cause 12 out of the 288 words in the multiframe to have 9 bits (see Fig.2). Six of these extra bits are '1's and six are '0's and after passing through the precoder, the extra bit being a '1' causes the 9th bit of the word to be different from the 8th bit and the reverse when the extra bit is a '0'. This situation is summarized in Table 3.

A major difficulty is now encountered because some of the words are 9 bits in length instead of 8. This implies that the binary data sequence, $\{c_n\}$, (see Fig.3) is no longer uniformly spaced in time. In general, when the idle states are not equiprobable and the sequence, $\{c_n\}$, becomes correlated as in equation (10), the calculation of the average autocorrelation function of the digital signal is extremely cumbersome and has not been attempted in this paper.

However, when the idle states are equiprobable, giving no correlation between the $\{c_n\}$, then the problems of the unequal spacing of the $\{c_n\}$ and the non-homogeneity of the idle code words disappear. This is because the members of a word pair are equiprobable and the inverse of each other; hence, when forming the autocorrelation function of the idling signal, non-zero contributions are obtained only from products of a word and its delayed version. This also means that the relative position of the different words

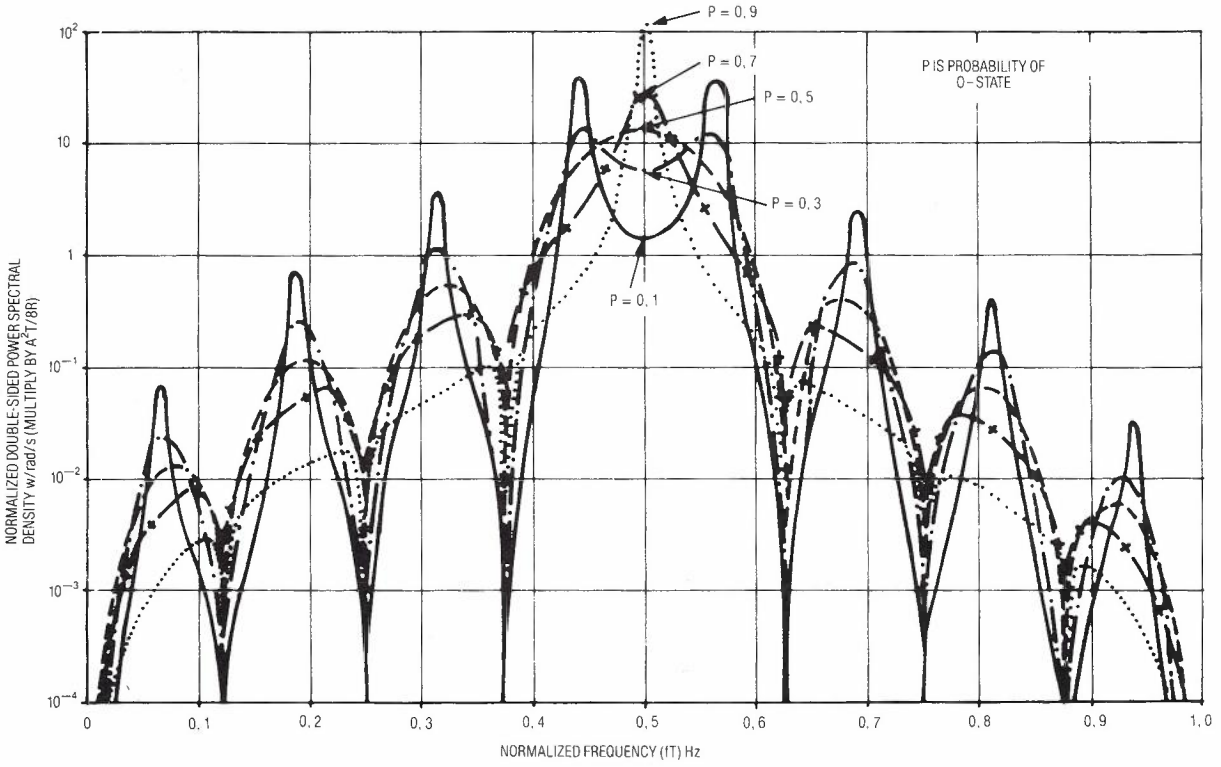

Fig. 5 - Power Spectral Densities of 24-Channel PCM Line Signal when Idling between 0+, 0- states for various probabilities of selection of the States.

TABLE 3 - List of Words After Precoder When Idling and Their Probabilities

No. of Bits/Word	Word Pair	Probability of Occurrence
8	-1 +1 -1 +1 -1 +1 -1 +1 +1 -1 +1 -1 +1 -1 +1 -1	276/288
9	-1 +1 -1 +1 -1 +1 -1 +1 -1 +1 -1 +1 -1 +1 -1 +1 -1 +1	6/288 (last word in frame with 193rd bit '1')
9	-1 +1 -1 +1 -1 +1 -1 +1 +1 +1 -1 +1 -1 +1 -1 +1 -1 -1	6/288 (last word in frame with 193rd bit '0')

in Table 3 is not relevant. In short, to evaluate the average power spectrum with equiprobable idling states, we need only evaluate the power spectra of the individual words in Table 3 and multiply them by their respective probabilities.

The Fourier Transform of the first word in Table 3 has already been given (see equation (19)) and the Fourier Transforms for the next two words are:

$$W_2(\omega) = 1 - e^{+j\omega T} - e^{-j\omega T} + e^{j\omega 2T} + e^{-j\omega 2T} - e^{j\omega 3T} - e^{-j\omega 3T} + e^{j\omega 4T} + e^{-j\omega 4T}$$

$$= 1+2(-\cos\omega T + \cos 2\omega T - \cos 3\omega T + \cos 4\omega T) \qquad (21)$$

and

$$W_3(\omega) = 1 - e^{j\omega T} - e^{-j\omega T} + e^{j\omega 2T} + e^{-j\omega 2T} - e^{j\omega 3T} - e^{-j\omega 3T} + e^{j\omega 4T} - e^{-j\omega 4T}$$

$$= 1+2(-\cos\omega T + \cos 2\omega T - \cos 3\omega T) + j2\sin 4\omega T, \qquad (22)$$

and the resulting average power spectrum becomes

$$P(\omega) = \frac{1}{8T}\,\frac{192}{193}\,\frac{1}{R}\,\frac{A^2T^2}{16}\left[\frac{\sin\omega T/4}{\omega T/4}\right]^2 4\sin^2\omega T/2$$

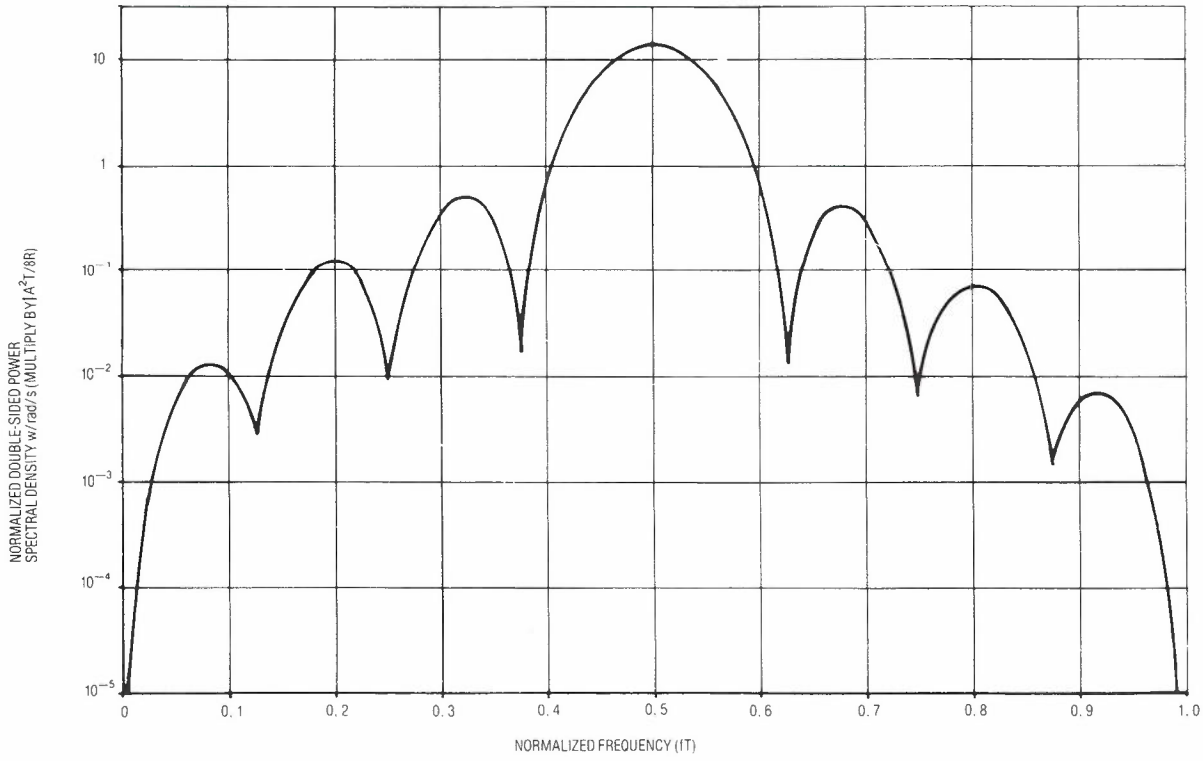

Fig. 6 - Power Spectral Density of 24-Channel PCM Line Signal when Idling between 0+, 0- States with equal probability and including the effect of the 193rd bit.

$$\cdot\ 4\left[\frac{276}{288}\ (\sin\omega T/2 - \sin 3\omega T/2 + \sin 5\omega T/2 - \sin 7\omega T/2)^2\right.$$

$$+\ \frac{6}{288}\ (0.5 - \cos\omega T + \cos 2\omega T - \cos 3\omega T + \cos 4\omega T)^2$$

$$\left.+\ \frac{6}{288}\ \{(0.5 - \cos\omega T + \cos 2\omega T - \cos 3\omega T)^2 + \sin^2 4\omega T\}\right] \qquad (23)$$

and is plotted in Fig.6. As expected, the effect of the 193rd bit is small (compare Figs.6 and 5 (p = 0.5)).

5.2 Random Selection of Other Idle Code Pairs

As stated in Section 4, offset voltages in the PCM encoder can cause the idling levels to be other than the two zero levels. In this part of the paper we consider various pairs of adjacent idle codewords (see Table 2) and determine the resulting average power spectrum of the line signal when the two members of the pair are selected in a random equiprobable fashion. The idling code pairs chosen for analysis are shown in Table 4. Table 4 also indicates the output word from the precoder which is multiplied by ± 1 on an equiprobable basis.

The derivation of the power spectra for the various cases in Table 4 follows the method outlined in part 5.1 of this Section of the paper, except for the idle code pairs 1,2 and -1,-2, which because they differ between each other in two bits, then have a periodic component in their idling signal as well as a random component. The spectra of the random components are shown in Fig.7, while the power of the discrete frequency components in the idle code pairs 1,2 and -1,-2 are shown in Fig.8. The above spectra assume equal probabilities between the idle code-words; if the probability is unequal, the spectral densities of the random components should be multiplied by

$$\frac{4p(1-p)}{1 + 2\cos 8\omega T(2p - 1) + (2p - 1)^2}$$

as in equation (20).

6. CALCULATION OF POWER IN A GIVEN BANDWIDTH

The power in a given bandwidth can be derived from the power spectral densities as follows:

TABLE 4 - Precoder Output Code Words for Various Idle Code Pairs Close to the Zero Level

Idle Code Pairs (refer to Table 2 for definition)	Output Word from Precoder and Associated Fourier Transform
3, 2	1 -1 1 -1 1 -1 1 1
	Fourier Transform:
	$2\cos 7\omega T/2 + j2(\sin\omega T/2 - \sin 3\omega T/2 + \sin 5\omega T/2)$
2, 1	Deterministic Component (period 16T):
	1 -1 1 -1 1 -1 0 1 -1 1 -1 1 -1 1 0 -1
	Random Component: ± 1 every 8T
1, 0+	same as 0+, 0- case
0+, 0-	1 -1 1 -1 1 -1 1 -1
	Fourier Transform: see equation (19)
0-, -1	same as 3, 2 case
-1, -2	Deterministic Component (period 8T)
	1 -1 1 -1 1 -1 0 1
	Random Component: $\pm$ every 8T
-2, -3	1 1 -1 1 -1 1 -1 -1
	Fourier Transform:
	$j2(\sin\omega T/2 - \sin 3\omega T/2 + \sin 5\omega T/2 + \sin 7\omega T/2)$

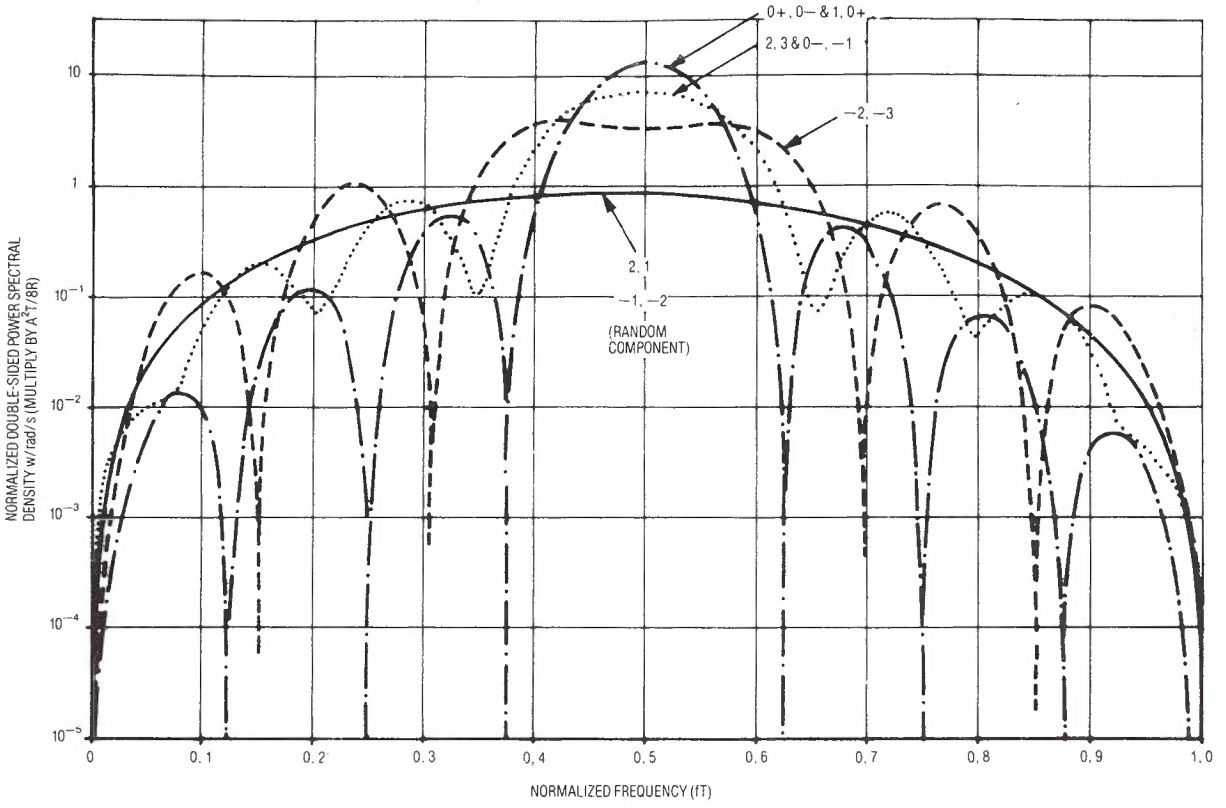

Fig. 7 - Power Spectral Densities of 24-Channel PCM Line Signal when Idling with equal probability between various pairs of States adjacent to the Zero States.

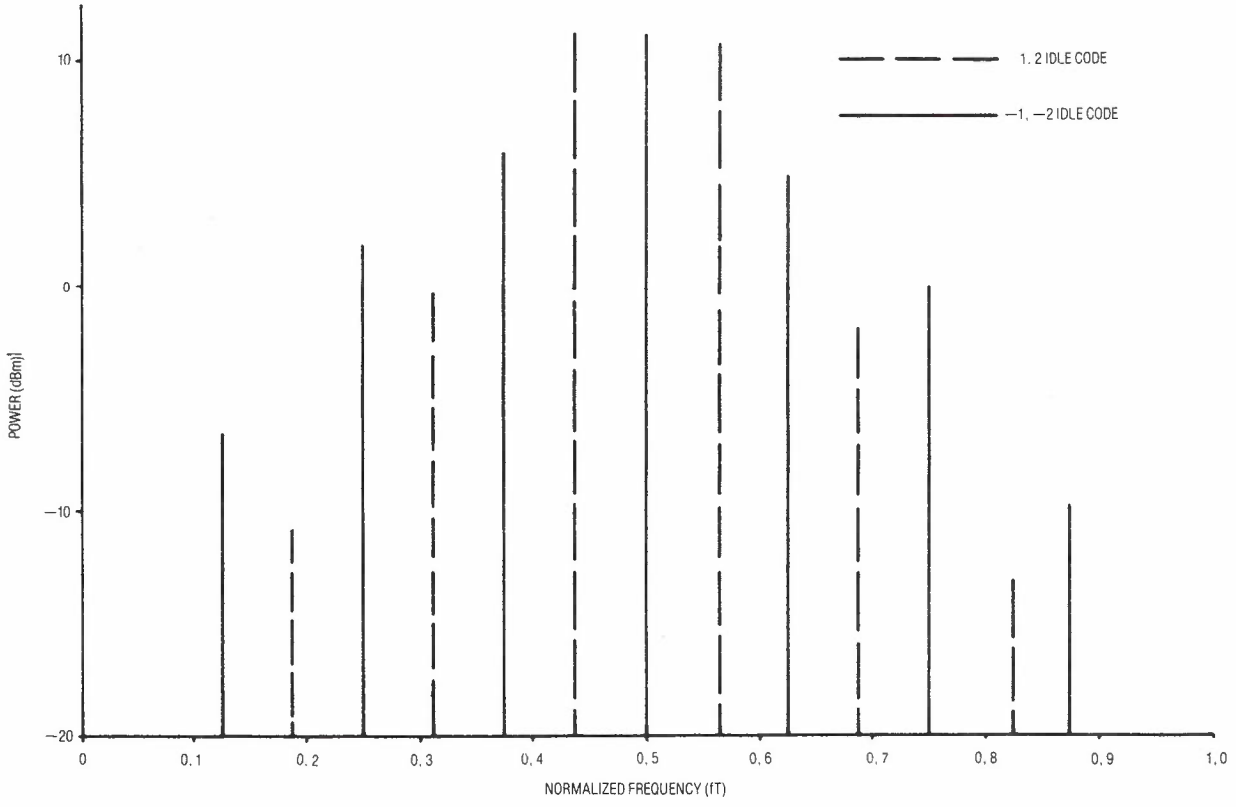

Fig. 8 - Power at Various Frequencies of a 24-Channel PCM Line Signal when Idling with equal probability between the 1, 2 and -1, -2 pairs.

$$P_T = \frac{1}{R}\frac{1}{2\pi} 2\int_{\omega_1}^{\omega_2} P(\omega)\, d\omega \qquad (24)$$

where P_T is the power in the frequency band between ω_1 and ω_2 rad/s and R is the resistance. The factor 2 is required because $P(\omega)$ is a double sided spectral density.

As an example, consider the maximum power in a 4kHz bandwidth of the PCM signal when idling with equal probability between the two zero states. This value is important in studies of the cross-talk interference of PCM signals into FDM systems. Assuming the power spectral density is nearly flat near the maximum, the maximum power in a 4kHz bandwidth is

$$P_{Tmax} = \frac{1}{R}\frac{1}{2\pi} 2P(\omega)_{max}\, 2\pi 4.10^3.10^3 \text{ mW} \qquad (25)$$

and on substituting A = 3, R = 110 and T = $(1.544.10^6)^{-1}$ into (23) and (25) we obtain

$$P_{Tmax} = -1.6 \text{ dBm} \qquad (26)$$

If this signal is psophometrically weighted, a further correction of -3.6dBm, (Ref.6), can be applied to give -5.4dBmp. This should be compared with a value of -14.2dBmp which is obtained when the PCM signal is carrying random equiprobable data signals. This example highlights the need to consider the idling condition as well as the random data condition of the PCM signal when carrying out performance studies.

7. CONCLUSION

In this paper we have considered the line signal of the 24-channel PCM system when in the idling condition. From measurements of the idle states of each channel in a PCM system, we conclude that a complete description of the resulting line signal would be very complicated; instead, we have formed an idealized model of the PCM system when idling. This model includes the effect of unequal probabilities of selection between two idle states and also the effect of offsets in the PCM encoder which determines the idle states.

Except in a few cases, the power spectrum of the line signal when in the idle condition, as determined from the idealized model, is continuous and is significantly more concentrated near the maximum than when carrying random digital signals. In addition, the effect of unequal probabilities of selection of the idle states has a significant effect on the shape of the spectrum.

8. ACKNOWLEDGEMENT

The author would like to thank G. Semple, J. Park, R. Coutts and Dr. A. Gibbs for their helpful discussions.

9. REFERENCES

1. CCITT Recommendation G.711, "Pulse Code Modulation (PCM) of Voice Frequencies", CCITT Green Book, Vol.III-2, Line Transmission, I.T.U. Geneva 1973.

2. CCITT Recommendation G.733, "Characteristics of Primary PCM Multiplex Equipment Operating at 1544 kbit/s", CCITT Green Book, Vol. III-2, Line Transmission, I.T.U. Geneva 1973.

3. Croisier, A., "Introduction to Pseudoternary Transmission Codes". IBM J. of Res. and Dev., Vol.14, pp.354-367, July 1970.

4. Duc, N.Q. and Smith, B.M., "Line Coding for Digital Data Transmission", Australian Telecommunications Research. Vol.11, No.2, 1977. pp.14-27.

5. Franks, L.E., "Signal Theory", Prentice-Hall Inc., Englewood Cliffs, New Jersey, U.S.A., 1969.

6. CCITT Recommendation G.223, "Assumptions for the Calculation of Noise on Hypothetical Reference Circuits for Telephony", CCITT Green Book, Vol.III-1, Line Transmission, I.T.U. Geneva 1973.

APPENDIX

Channel Number	Idle Words (Sign Bit MSB … LSB)	Idle Levels	Frequency of Occurrence
1	1 1 1 1 1 1 1 0	+1	4/32
	1 1 1 1 1 1 1 1	0+	23/32
	0 1 1 1 1 1 1 1	0−	5/32
2	1 1 1 1 1 1 1 1	0+	32/32
3	1 1 1 1 1 1 1 0	+1	1/32
	1 1 1 1 1 1 1 1	0+	18/32
	0 1 1 1 1 1 1 1	0−	13/32
4	1 1 1 1 1 1 1 1	0+	18/32
	0 1 1 1 1 1 1 1	0−	14/32
5	1 1 1 1 1 1 1 0	+1	3/32
	1 1 1 1 1 1 1 1	0+	29/32
6	1 1 1 1 1 1 1 0	+1	1/32
	1 1 1 1 1 1 1 1	0+	26/32
	0 1 1 1 1 1 1 1	0−	5/32
7	1 1 1 1 1 1 1 0	+1	30/32
	1 1 1 1 1 1 1 1	0+	2/32
8	1 1 1 1 1 1 0 1	+2	1/32
	1 1 1 1 1 1 1 0	+1	31/32
9	1 1 1 1 1 1 0 1	+2	11/32
	1 1 1 1 1 1 1 0	+1	21/32
10	1 1 1 1 1 1 0 0	+3	1/32
	1 1 1 1 1 1 0 1	+2	15/32
	1 1 1 1 1 1 1 0	+1	5/32
	1 1 1 1 1 1 1 1	0+	11/32
11	1 1 1 1 1 0 1 1	+4	15/32
	1 1 1 1 1 1 0 0	+3	17/32
12	1 1 1 1 1 1 1 0	+1	15/32
	0 1 1 1 1 1 1 1	0−	5/32
	0 1 1 1 1 1 1 0	−1	12/32
13	1 1 1 1 1 1 1 0	+1	13/32
	1 1 1 1 1 1 1 1	0+	19/32
14	1 1 1 1 1 1 0 1	+2	1/32
	1 1 1 1 1 1 1 0	+1	30/32
	1 1 1 1 1 1 1 1	0+	1/32
15	1 1 1 1 1 0 1 1	+4	1/32
	1 1 1 1 1 1 0 0	+3	2/32
	1 1 1 1 1 1 0 1	+2	24/32
	1 1 1 1 1 1 1 0	+1	5/32
16	1 1 1 1 1 1 0 0	+3	1/32
	1 1 1 1 1 1 0 1	+2	30/32
	1 1 1 1 1 1 1 0	+1	1/32
17	1 1 1 1 1 1 0 0	+3	25/32
	1 1 1 1 1 1 0 1	+2	5/32
	1 1 1 1 1 1 1 0	+1	2/32
18	1 1 1 1 1 1 0 0	+3	29/32
	1 1 1 1 1 1 0 1	+2	3/32

Channel Number	Idle Words								Idle Levels	Frequency of Occurrence
	Sign Bit	MSB						LSB		
19	1	1	1	1	1	0	1	1	+4	1/32
	1	1	1	1	1	1	0	0	+3	26/32
	1	1	1	1	1	1	0	1	+2	5/32
20	1	1	1	1	1	1	0	1	+2	29/32
	1	1	1	1	1	1	1	1	0+	1/32
	0	1	1	1	1	1	1	1	0-	2/32
21	1	1	1	1	1	0	0	1	+6	1/32
	1	1	1	1	1	0	1	0	+5	3/32
	1	1	1	1	1	0	1	1	+4	23/32
	1	1	1	1	1	1	0	0	+3	5/32
22	1	1	1	1	1	1	0	0	+3	1/32
	1	1	1	1	1	1	0	1	+2	3/32
	1	1	1	1	1	1	1	1	0+	1/32
	0	1	1	1	1	1	1	1	0-	27/32
23	1	1	1	1	1	1	0	0	+3	31/32
	1	1	1	1	1	1	1	0	+1	1/32
24	1	1	1	1	1	1	0	0	+3	1/32
	1	1	1	1	1	1	0	1	+2	6/32
	1	1	1	1	1	1	1	1	0+	25/32

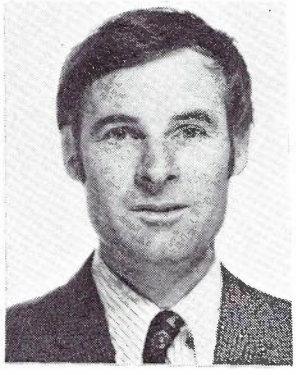

BIOGRAPHY

BERNARD SMITH was born in Mt. Gambier, South Australia, and studied Electrical Engineering at the University of Adelaide where he obtained the degrees of Bachelor of Engineering (Honours) in 1964 and Doctor of Philosophy in 1969. He joined the Research Laboratories of Telecom Australia in 1968 where he is currently an Engineer Class 4 (Acting) in the Transmission Systems Branch. Whilst working in the Research Laboratories, he has been concerned with various problems in line transmission systems and in particular digital data transmission at all speeds in the telephone network.

Book Review

Sequency Theory; Foundations And Applications
by H. F. Harmuth (Academic Press, New York, 1977)

Research into communications applications for Walsh function techniques has continued vigorously since interest was generated, largely by Harmuth, in 1969. This book continues in the deep, exhaustive style of Harmuth's earlier work. In this work, Harmuth has concentrated on a number of areas of communications research and quantum physics which are well proven applications for sequency techniques. Many other areas of communications and electronics research where Walsh functions are under investigation have not been considered in this work. The emphasis here is on filtering and processing of signals for television and underwater acoustic imaging, electromagnetic propagation for radar applications, and mathematical applications in quantum physics.

The first chapter treats the mathematical foundations required for the application of Walsh functions to signal and waveform processing. A comparison is drawn between Fourier and Walsh - Fourier techniques, followed by a consideration of fast transforms and various dyadic operations commonly used in sequency analysis. The treatment is exhaustive and lucid but requires a high level of mathematical understanding. Diagrams and charts are used very effectively in this part of the work to aid the understanding of some difficult concepts. This introductory, mathematical treatment is handled more lucidly than in Harmuth's first book, (Ref.1).

The remaining chapters specialise in particular applications. Chapters two and three concentrate on communications system applications and chapter four on the applied mathematics of quantum physics. This final chapter is particularly heavy going and is of little interest to telecommunication engineers.

The communication applications are treated with an admirable balance between mathematical theory and practical design. Waveforms and circuit diagrams are used freely throughout as well as occasional photographs of laboratory equipment. All these factors lead to a readable, although conceptually complex account of recent work which is not widely known. The circuit realisations used throughout chapter two are basic indeed, however they are used effectively to bring the reader closer to practicalities. For example, the detailed discussion of generators for time-variable Walsh functions based on recurrence relations is of academic interest only when it is considered that cheaper, more reliable designs may be achieved with a simple counter and semiconductor memory. However, the author obviously has a keen awareness of technology developments when discussing the practicability of two and three dimensional filters for imaging.

The discussion of general electromagnetic wave effects in chapter three is practically oriented and leads on well to the treatment of practical radiators, receivers and radar applications. The author has been a leader in research into antennae and antenna array design for orthogonal time signals, and over one hundred pages of the book bear this out. Improvements in the resolution of radar arrays may be achieved using sequency techniques; therefore Harmuth's work should be of interest to researchers in this field.

In summary, Sequency Theory is an up-to-date account of proven research techniques in the above fields. Although the field of orthogonal functions in communications is filled with new concepts, sometimes rather complex, the author's treatment is lucid and exhaustive at the same time. The book is likely to be useful to post-graduate researchers in the fields of signal processing and analysis, electromagnetic propagation for radar, acoustics and theoretical physics. The bibliography is extensive and useful to all workers in the Walsh function field. This book is not recommended as a basic introduction to Walsh functions and sequency techniques.

REFERENCE

1. Harmuth, H. F., "Transmission of Information by Orthogonal Functions", Springer Verlag, New York, 2nd edition, 1972.

P.S. Jones
Telecom Australia
Research Laboratories.

Printed by Standard Newspapers Limited, 10-14 Park Road, Cheltenham, 3192.

AUSTRALIAN
TELECOMMUNICATION
RESEARCH

VOLUME 11, NUMBER 3,
1977

Contents*

*Abbreviated Titles